

Electrochemical Detection of Chemical Warfare Agents

A Thesis Submitted to the
College of Graduate Studies and Research
in Partial Fulfillment of the Requirements
for the degree of Masters of Science
in the Department of Chemistry
University of Saskatchewan
Saskatoon

By

Mohammad Abdul Kader Khan

Permission to Use

In presenting this thesis, in partial fulfillment to the requirements for the degree of Masters of Science from the University of Saskatchewan, I agree that the libraries of this University may make it freely available for inspection. I further agree that permission for copying of this thesis in any manner, in whole or in part, for scholarly purposes may be granted by the professors who supervised my thesis work or, in their absence, by the Head of the Department of Chemistry, or the Dean of the College of Graduate Studies and Research. It is understood that any copying or publication or use of this thesis or parts thereof, for financial gain shall not be allowed without my written permission. It is also understood that due recognition shall be given to me and to the University of Saskatchewan in any scholarly use which may be made of any material in this thesis.

Request for permission to copy or to make other use of material in this thesis in whole or in part should be addressed to:

Head of the Department of Chemistry

University Of Saskatchewan

Saskatoon, Saskatchewan

S7N 5C9

Abstract

tert-butyl 1'-methoxycarbonyl-1-ferrocenecarbamate, Boc-NH-Fc-COOMe, (**1**) was synthesized according to the literature procedure and modified to 1-amino-*n'*-ferrocenemethylcarboxylate, 1,*n'*-H₂N-Fc-COOCH₃ (**2**) by removing the Boc-group with TFA/Et₃N mixture in dichloromethane. Compound **2** reacted with alkylating agents like MeI, EtI, EtSCH₂CH₂Cl (MA) and (CN)(EtO)₂P(O) (NA) to form MeNH-Fc-COOMe (**3**), EtNH-Fc-COOMe (**4**), EtSCH₂CH₂NH-Fc-COOMe (**5**), (EtO)₂P(O)NH-Fc-COOMe (**6**), respectively. Cyclic voltammetry (CV) of these compounds showed different half-wave potential characteristics compared to aminoferrocene and was dependent on the nature of the substituents, which was rationalized by molecular orbital calculations. Electron donating groups (Me, Et and 2-chloroethyl ethylsulfide, MA) shifted the half-wave potential towards the cathodic direction while electron withdrawing group like diethyl cyanophosphonate, NA, shifted it toward anodic direction. Anodic to cathodic peak separation were found to be within 62-88 mV indicating a quasi-reversible system.

Hydrolysis of compound **1** resulted in the formation of *tert*-butyl 1'-methoxycarbonyl-1-ferrocenecarboxylic acid, Boc-NH-Fc-COOH, (**11**) which was coupled with cystamine using the EDC/HOBt protocol to synthesize the cystamine conjugate [BocHN-Fc-CO-CSA]₂ (**12**). This molecule is equipped with an amino group that directly linked to the redox receptor. Compound **12** was fully characterized by spectroscopic methods and by single crystal x-ray diffraction. The cystamine conjugate **12** formed films on gold substrates, which upon deprotection of the amino group,

reacted with chemical warfare agents (CWAs) mimics, such as EtSCH₂CH₂Cl (MA), a simulant for the sulfur mustard HD, and (CN)(EtO)₂P(O) (NA), a simulant for the nerve agent Tabun. Their reaction with the surface-bound ferrocene derivative results in the formation of N-substituted products.

CV measurements showed anodic shifts of the Fc redox potentials by 50 (±5) mV after exposure to MA, and NA. Measurements by quartz crystal microbalance (QCM) showed an increase in mass upon exposure to MA and NA. Ellipsometry measured a film thickness increase from 6 (±1) Å for the deprotected film to 10 (±4) Å for the film modified with MA and to 7 (±2) Å for the film modified with NA. The surfaces were analyzed by x-ray photoelectron spectroscopy (XPS) and clearly showed the attachment of the cystamine conjugate on the surface and its reaction with CWAs mimics.

Acknowledgements

All praises are due to Allah, the Most-Beneficent and the Most-Merciful. With Him, the glory and success – and He bestow these to whomever He wants. I thank Him for all those He gave me and bring me up to this.

I would like to thank Dr. H.–B. Kraatz for giving me the opportunity to complete my Masters of Science degree with him. I must mention that I learn a lot from him not only in the area of chemistry but also in many other areas. He shared his vast knowledge with us in a very friendly manner.

I also want to thank my committee members Dr. Matthew F. Paige, Dr. Jens Mueller and Dr. Yuanming Pan for the advice, criticism and support during my research. I would like to appreciate all the past and present Kraatz group members – postdoctoral fellows namely Todd C Sutherland, Yi-Tao Long, Younian Liu, Subrata K. Dey, Yinglin Zhou, Xiaohong Li, Erfan Abu Irhayem, Donald Thomas, Thara Vasanth, Kegan Kerman and graduate students namely Francis Appoh, Dusmanti Jayasinghe, Yingshen Lu, Somenath Chowdhury, Khaled Mahmoud, Himadri Mandal, Grzegorz Orłowski, Haifeng Song, Mark Milne, Amir Kavianpour, Anas Lataifeh, Regan Wilks, Armando Marengo and undergraduate students namely Demyan Prokopchuk, Marek Majewski Jr., Adam Leontowich and Nancy Bawa.

I would like to thank Dr. Keith Brown and Dr. Gabriele Schatte for helping in NMR and specially Gabriele for X-ray crystallography. I would also like to thank Ken Thoms for collecting mass spectra and elemental analysis for the compounds. My sincere thanks to Dr. Dimitri Karpuzov at the University of Alberta in Edmonton for running X-ray photoelectron study on the samples I sent.

I am grateful to NATO, NSERC, Department of National Defense and Foreign Affairs and International Trade Canada for providing financial support for this project.

Finally, I want to express my gratitude to my parents. Without their encouragement and support, it would not have been possible for me to come up to this. My sincere thanks to my brother and sister and my wife for giving me company all the way and help me overcome difficulties and pain.

Dedication

This work is dedicated to those who spent their lives for the sake of truth, right path and guidance – who are our everlasting source of hope and inspiration to strive for the best.

Table of Contents

Permission to Use	i
ABSTRACT	ii
ACKNOWLEDGEMENTS	iv
DEDICATION	vi
TABLE OF CONTENTS	vii
LIST OF TABLES	xi
LIST OF FIGURES	xii
LIST OF SCHEMES	xvi
LIST OF CHARTS	xviii
LIST OF ABBREVIATIONS	xix
LIST OF SYMBOLS	xxii
LIST OF COMPOUNDS	xxiii
1. Introduction	1
1.1. What is a Chemical Warfare Agent?	1
1.2. Chemical Warfare Agents in the Environment	3
1.3. Toxicities of CWAs and Their Hydrolysis Products	5
1.4. Present Detection Technologies	6
1.5. Electrochemical Sensors	7
1.5.1. Solution-Phase Electrochemical Sensors for CWAs	8
1.5.2. Solid-Phase Electrochemical Sensors for CWAs	11
1.6. Objectives and Research Proposal	20

2. Reactions of 1-Amino- <i>n'</i> -Ferrocenemethylcarboxylate with Electrophiles: A Combined Synthetic, Electrochemical, and Theoretical Study	22
2.1. Synthesis and Characterization	22
2.2. Electrochemical Study	25
2.3. Quantum Mechanical Calculations	27
3. Surface Studies of Amino Ferrocene Derivatives on Gold: Towards Electrochemical Sensors for Chemical Warfare Agents	29
3.1. Synthesis and Characterization	29
3.2. Surface Studies	34
3.2.1. Cyclic Voltammetry	34
3.2.2. Differential Pulse Voltammetry	37
3.2.3. Surface Titration	38
3.2.4. Quartz Crystal Microbalance	39
3.2.5. X-ray Photoelectron Spectroscopy	41
4. Conclusions and Future Research	45
4.1 Conclusions	45
4.2 Future Research	45
5. Experimental	48
5.1. General Remarks	48
5.2. General Synthetic Method for Compounds 3 – 6	49
5.2.1. Synthesis and Characterization of 1, <i>n'</i> -MeHN-Fc-COOMe (3) ..	50
5.2.2. Synthesis and Characterization of 1, <i>n'</i> -EtHN-Fc-COOMe (4) ..	51

5.2.3. Synthesis and Characterization of 1, <i>n'</i> -EtSCH ₂ CH ₂ HN-Fc-COOMe (5)	52
5.2.4. Synthesis and Characterization of 1, <i>n'</i> -(EtO) ₂ P(O)NH-Fc-COOMe (6)	53
5.2.5. Synthesis and Characterization of [BocNH-Fc-CO-CSA] ₂ (12)	54
5.3. Electrochemical Measurements	55
5.4. Quantum mechanical Calculations	55
5.5. Film Preparation and Surface Electrochemistry	56
5.6. Ellipsometry Study	57
5.7. Quartz Crystal Microbalance Measurements	57
5.8. X-ray Photoelectron Spectroscopy	58
5.9. X-ray crystallography	59
References	62
Appendix	70
Figure A1: ¹ H-NMR spectrum of 1, <i>n'</i> -NH ₂ -Fc-COOMe (2) in CDCl ₃ at room temperature with full peak assignment.	70
Figure A2: ¹ H-NMR spectrum of 1, <i>n'</i> -MeHN-Fc-COOMe (3) in CDCl ₃ at room temperature with full peak assignment.	70
Figure A3: ¹ H-NMR spectrum of 1, <i>n'</i> -EtHN-Fc-COOMe (4) in CDCl ₃ at room temperature with full peak assignment.	71
Figure A4: ¹ H-NMR spectrum of 1, <i>n'</i> -EtSCH ₂ CH ₂ HN-Fc-COOMe (5) in CDCl ₃ at room temperature with full peak assignment.	71

Figure A5: ^{31}P -NMR spectrum of 1, <i>n'</i> -(EtO) $_2\text{P}(\text{O})\text{NH-Fc-COOMe}$ (6) in MeOD at room temperature.	72
Figure A6: UV-visible spectrum of [BocNH-Fc-CO-CSA] $_2$ (12) in CH $_3\text{CN}$ at room temperature.	72
Figure A7: Partial IR spectrum of [BocNH-Fc-CO-CSA] $_2$ (12) in KBr at room temperature with band assignment.	73
Figure A8: RAIRS spectrum of [BocNH-Fc-CO-CSA] $_2$ (12) on Au surface immobilized by soaking at room temperature from 1 mM ethanolic solution of compound 12	74
Table A1: Interatomic Distances [\AA] of compound 12	75
Table A2: Interatomic Angles [$^\circ$] for compound 12	76
Copy right permission from Elsevier for Figure 1.1.	79
Copy right permission from American Chemical Society for Figure 1.2 – 1.6 and Scheme 1.6.	80

List of Tables

Table 1.1: Toxicity data for some common chemical warfare agents. Given are toxicities of the agents measured by concentration of the agent in air (LC ₅₀) and inhalational toxicity (LC _{t50}).	6
Table 2.1: Selective spectroscopic data for compounds 3–6	24
Table 2.2: CV parameters for compounds 2–6 (solvent: CH ₃ CN, scan rate: 100 mV/s, working electrode: glassy carbon, reference electrode: Ag/AgCl, counter electrode: Pt wire, electrolyte: 0.2 M TBAP)	26
Table 3.1: Selected bond distances (in Å) and bond angles (in °) for compound 12	33
Table 3.2: D(H)···A distances (in Å) for compound 12	33
Table 3.3: Electrochemical parameters and thicknesses of 12 on 25 μm gold electrodes and Au on Si substrates	38
Table 3.4: Frequency and mass changes on QCM after deprotection and exposure of 12-d to MA and NA	41
Table 3.5: N1s fitting values for compound 12 and modified films	44
Table 5.1: Crystal data and refinement of compound 12 × CHCl ₃	60

List of Figures

Figure 1.1:	(a) Reaction scheme showing electrocatalysis of DECP using electrochemically generated iodide ion. (b) CVs of NaI in the presence of DECP. 0.05 M NaClO ₄ , 0.05 M phosphate buffer (pH 6.3), 0.40 mM NaI. In (A), DECP (mM): a. 0 (solid curve), b. 0.02, c. 0.05, d. 0.10, e. 0.20, f. 0.30.	9
Figure 1.2:	Analysis of hydrolysis products of nerve agents MPA, IMPA and PMPA by capillary electrophoresis. pH 4.0; voltage, 30 kV (negative polarity).	10
Figure 1.3:	(i) Reaction scheme of OPH-catalyzed hydrolysis of organophosphate nerve agent (A) followed by electrooxidation of the liberated p-nitrophenol (B). (ii) Current-time amperometric response to successive increments of organophosphorus pesticides paraoxon. Insets: calibration plots for paraoxon.	14
Figure 1.4:	Schematics of layer-by-layer electrostatic self-assembly of AChE onto carbon nanotube: (A) assembling positively charged PDDA on negatively charged nanotube; (B) assembling negatively charged AChE; (C) assembling the second PDDA layer.	15

Figure 1.5:	(a) Typical amperometric responses of PDDA/AChE/PDDA/nanotube/glassy carbon biosensor during the flow injection analysis of organophosphorus pesticide, paraoxon. Signals 1 and 2, initial enzyme activity; signals 3 and 4, after incubating 6 min with 0.1 nM paraoxon; signals 5 and 6, after regeneration; signals 7 and 8, after incubating 6 min with 10 nM paraoxon. (b) Inhibition curve of the PDDA/AChE/PDDA/nanotube/glassy carbon biosensor to different concentrations of paraoxon.	16
Figure 1.6:	Potentiometric responses of the MPA cavity sensor for MPA. [MPA](CHCl ₃ /CCl ₄) = 2.5 × 10 ⁻² M; [octadecyltrichlorosilane] = 8.0 × 10 ⁻⁴ M. Adsorption time 3 min.	18
Figure 2.1:	Cyclic voltammetry of compounds 2 and 6 in CH ₃ CN solution with glassy carbon electrode as working electrode, Pt wire as counter electrode and Ag/AgCl as reference electrode and 0.2 M tetrabutylammonium perchlorate (TBAP) as supporting electrolyte with a scan rate of 100 mV/s.	25
Figure 2.2:	HOMO contours and energies of compounds 2–6	28
Figure 3.1:	(a) ¹ H-NMR spectrum of [(BocNH)Fc(CO)CSA] ₂ (12) and (b) ¹³ C-NMR spectrum of [(BocNH)Fc(CO)CSA] ₂ (12) in CDCl ₃	31
Figure 3.2:	(a) ORTEP plot of [BocNH(C ₅ H ₄)Fe(C ₅ H ₄)C(O)NHCH ₂ CH ₂ S] ₂ (12) shown at the 30% probability level. (b) 1,5' conformation of Fc1 (c) 1,1' conformation of Fc2 with respect to the orientation of the substituents. H-atoms are omitted for clarity.	32

Figure 3.3:	(a) CVs of 25 μm gold microelectrode surfaces modified with 12 (solid line) and deprotected 12-d (\circ). (b) 12-d after exposure to 1 ppm MA, (12-d+MA) (\circ) and NA, 12-d+NA (solid line) in 2.0 M NaClO_4 solution. Scan rate 100 V/s, reference electrode Ag/AgCl (3M KCl) and counter electrode Pt wire.	36
Figure 3.4:	(a) DPVs of 25 μm gold microelectrode surfaces modified with 12 (solid line) and deprotected 12-d (\circ). (b) 12-d after exposure to 1 ppm MA, (12-d+MA) (solid line) and NA, 12-d+NA (\circ) in 2.0 M NaClO_4 solution. Amplitude: 0.05 V, pulse width: 0.05 sec and pulse period: 0.2 sec.	37
Figure 3.5:	(a) Changes in potential on addition of increasing concentration of MA and (b) NA to surface immobilized 12-d . Working electrode: gold microelectrode (25 μm diameter); reference electrode: Ag/AgCl; counter electrode: Pt wire; electrolyte: 2M NaClO_4 ; scan rate: 100V/s.	38
Figure 3.6:	Typical QCM plot for frequency changes (Δf) vs. time of the Au surfaces on quartz crystal modified with 12 (\circ), deprotected 12-d (\circ), 12-d+MA (\square) and 12-d+NA (\diamond) at 25 $^\circ\text{C}$	40
Figure 3.7:	XPS S 2p spectra for (a) 12 (b) 12-d+MA and Fe 2p spectra for (c) 12 and (d) 12-d+NA films on gold surface.	42
Figure 3.8:	XPS N1s spectra for (a) 12 (b) 12-d (c) 12-d+MA (d) 12-d+NA films on gold surface.	43

Figure A1:	^1H -NMR spectrum of 1, <i>n'</i> -NH ₂ -Fc-COOMe (2) in CDCl ₃ at room temperature with full peak assignment.	70
Figure A2:	^1H -NMR spectrum of 1, <i>n'</i> -MeHN-Fc-COOMe (3) in CDCl ₃ at room temperature with full peak assignment.	70
Figure A3:	^1H -NMR spectrum of 1, <i>n'</i> -EtHN-Fc-COOMe (4) in CDCl ₃ at room temperature with full peak assignment.	71
Figure A4:	^1H -NMR spectrum of 1, <i>n'</i> -EtSCH ₂ CH ₂ HN-Fc-COOMe (5) in CDCl ₃ at room temperature with full peak assignment.	71
Figure A5:	^{31}P NMR spectrum of 1, <i>n'</i> -(EtO) ₂ P(O)NH-Fc-COOMe (6) in MeOD at room temperature.	72
Figure A6:	UV-visible spectrum of [BocNH-Fc-CO-CSA] ₂ (12) in CH ₃ CN at room temperature.	72
Figure A7:	Partial IR spectrum of [BocNH-Fc-CO-CSA] ₂ (12) in KBr at room temperature with band assignment.	73
Figure A8:	RAIRS spectrum of [BocNH-Fc-CO-CSA] ₂ (12) on Au surface immobilized by soaking at room temperature from 1 mM ethanolic solution of compound 12	74

List of Schemes

Scheme 1.1: Hydrolysis of sulphur mustard, 2-dichloroethyl sulfide, HD.	4
Scheme 1.2: Hydrolysis of nerve agent VX to ethyleneiminium ion and of nerve agents sarin (GB) and soman (GD) to PMPA, IMPA and MPA.	4
Scheme 1.3: Different concepts for designing electrochemical sensor based on self-assembly. (A) self-assembly, (B) layer by layer assembly and (C) channel formation by self-assembly	12
Scheme 1.4: Reaction scheme of enzymatic sensor using AChE as enzyme for detecting organophosphorus pesticides.	16
Scheme 1.5: Formation of selective MPA cavities on ITO-coated glass plates.	18
Scheme 1.6: Scheme of electrochemical sensing of nitroaromatic organophosphorus pesticides. (A) Electrodeposition of zirconia nanoparticle to gold electrode surface; (B) nitroaromatic organophosphorus pesticides adsorb to zirconia nanoparticle surface; (C) electrochemical stripping detection of nitroaromatic organophosphorus pesticides; X = O or S and R = nitroaromatic organophosphorus pesticide group.	19
Scheme 2.1: Reactions of 2 with alkylating agents: (i) TFA in DCM, (ii) Et ₃ N, (iii) EtOH and (iv) saturated NaHCO ₃ ; 3 : R = Me, 4 :	23

	R = Et, 5 : R = CH ₂ CH ₂ SEt, 6 : R = (P=O)(OEt) ₂	
Scheme 3.1:	Synthesis of compound [(BocNH)Fc(CO)CSA] ₂ (12). (i) CH ₂ Cl ₂ , HOBt, EDC; (ii) Et ₃ N.	30
Scheme 3.2:	Schematic view of surface modifications of compound 8 (a) in solution (b) on surface (c) deprotection of 12 to 12-d (d) exposure of 12-d with 1 ppm MA , 12-d+MA and (e) exposure of 12-d with 1 ppm NA, 12-d+NA	34
Scheme 4.1:	Scheme for modification of present sensor compound. R = Boc- His, Boc-Trp, Boc-Asp, Boc-Glu, Boc-Gln, Boc-Asn and Boc- Cys.	46

List of Charts

Chart 1: Some common chemical warfare agents and mimics.	2
---	---

List of Abbreviations

AChE	acetylcholinesterase
AFM	atomic force microscopy
Cp	cyclopentadienyl
CSA	cystamine
CV	cyclic voltammetry
CWA	chemical warfare agents
DCM	dichloromethane
DECP	diethyl cyanophosphonate
DMBP	4,4'-dimethyl-2,2'-bipyridyl) and 1:2 Cu(II)–TMEDA (<i>N,N,N',N'</i> -tetramethylethylenediamine
DMMP	diethyl methylphosphonate
DPV	differential pulse voltammetry
$E_{1/2}$	halfwave potential (solution)
E^0	formal potential
ΔE	anodic to cathodic peak separation
EDC	1-(3-dimethylaminopropyl)-3-ethylcarbodiimide hydrochloride
ΔE_{fwhm}	Peak separation at full width at half-maximum
Fc	ferrocene
Δf	change in frequency
GA	tabun
GB	sarin

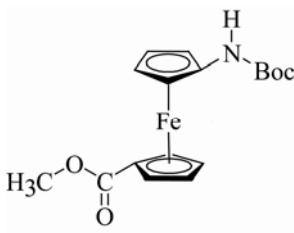
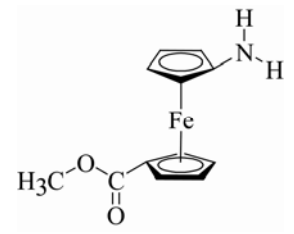
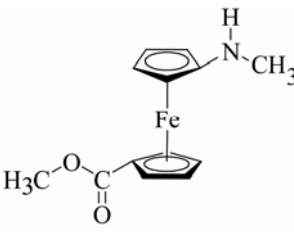
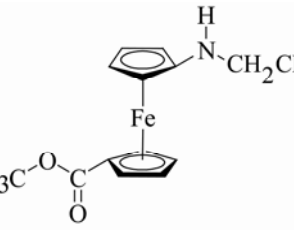
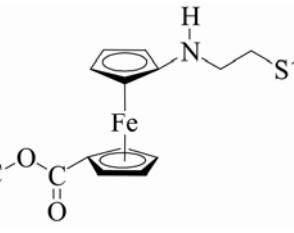
GD	soman
H	2-chloroethyl ethylsulfide
HOBt	1-Hydroxybenzotriazole hydrate
HOMO	highest occupied molecular orbital
IMPA	isopropyl methylphosphonic acid
ITO	indium tin oxide
LC ₅₀	the concentration of any agent in air necessary to kill 50% of the test subjects
LCt ₅₀	inhalational toxicity of the vapor of any agent in air necessary to kill 50% of the test subjects
LD ₅₀	lethal dose at which 50% of the population will die
MA	mustard gas HD simulant, 2-chloroethyl ethylsulfide
MPA	methyl phosphonic acid
NA	nerve agent Tabun simulant, diethyl cyanophosphonate
OPH	organophosphorus hydrolase
PDDA	poly(diallyldimethylammonium chloride)
PMPA	pinacolyl methylphosphonic acid
QCM	quartz crystal microbalance
SWNT	single-walled carbon nanotube
SWV	square wave voltammetry
TBAP	tetrabutylammonium perchlorate
TEM	transmission Electron Microscopy
TFA	trifluoroacetic acid

UPD under potential deposition
XPS x-ray photoelectron spectroscopy

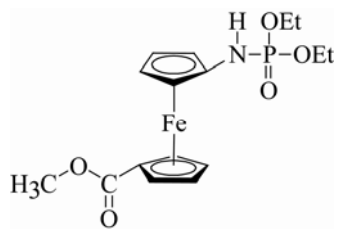
List of Symbols

μ	micron
η	hapticity
δ	chemical Shift
ε	extinction co-efficient
β	twist angles
ω	torsion angles
Γ	surface coverage
Δ	difference

List of Compounds

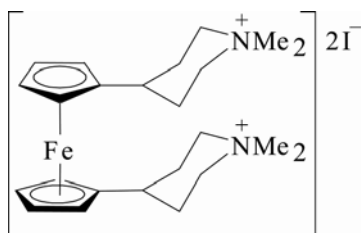
Number	Structure	Location in Thesis (page)
1		21,47,48
2		22-28,70
3		22-28,50,70
4		22-28,51,71
5		22-28,52, 71

6



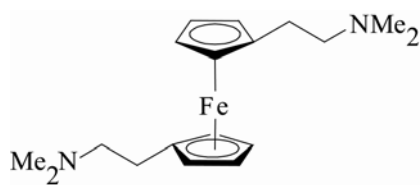
22-28,53, 72

7



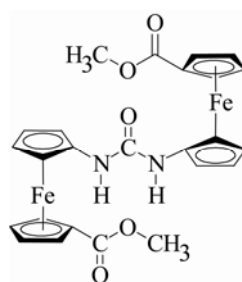
23

8



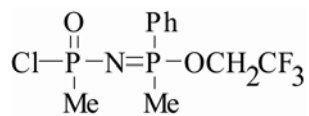
23

9



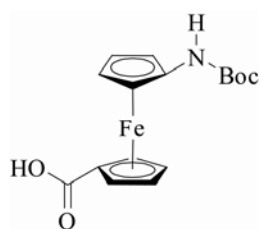
23

10

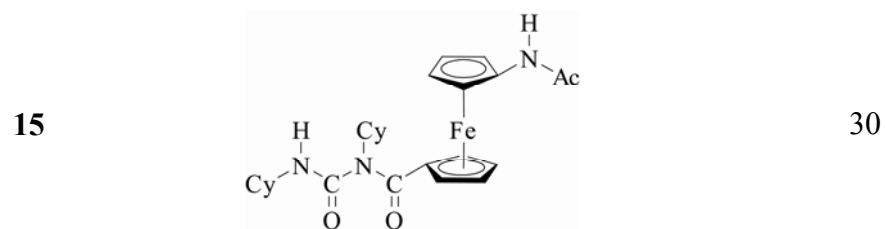
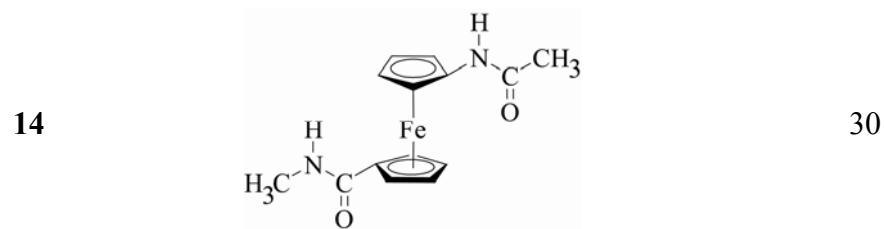
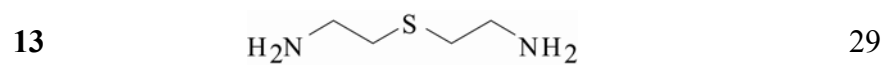
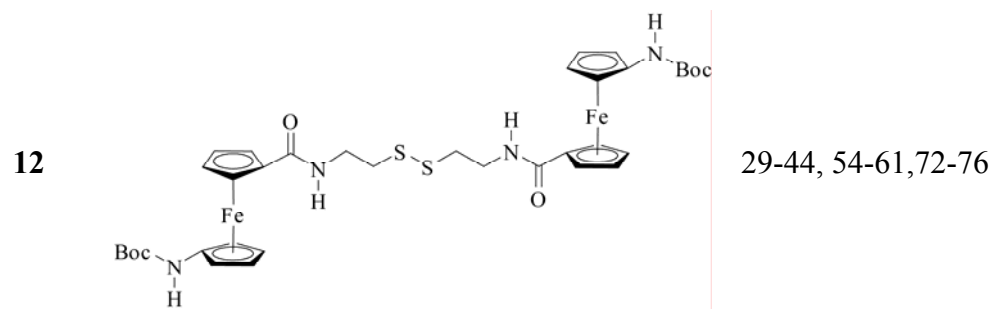


24

11



29,54



1. Introduction

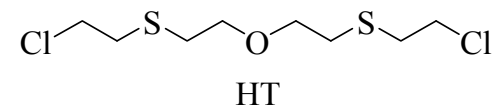
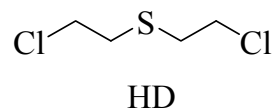
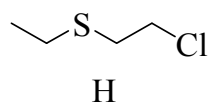
Chemical warfare agents (CWAs) are a growing concern to many countries. The uses of CWAs by terrorist, organizations or even states is significant as they can be readily synthesized by simple chemical reactions and often have an extremely high toxicity. Unfortunately, there is incidence of CWAs being used in human history and many countries. These chemicals were used on a large scale during the 1st World War and caused approximately 1.3 million casualties.¹ Sulfur mustards were used in 1980-1988 in the Iraq-Iran conflict being responsible for about 4% of all casualties.¹ Nerve agents were used against the Kurds in Iraq² and also in the terrorist attack on the Tokyo subway in 1995.³ Research into new CWAs, their production and use still continue in different areas around the world.⁴ Given the potential threat from these lethal agents, it is imperative to have an early warning system consisting of readily deployable sensors.

1.1. What is a Chemical Warfare Agent?

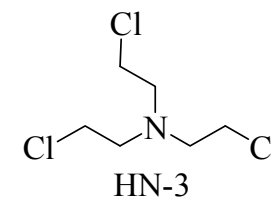
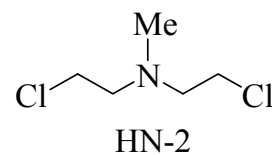
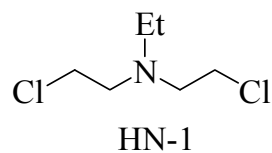
According to the “Biological and Toxic Weapons Conventions”⁵, CWAs are defined as “chemical substances, whether gaseous, liquid or solid, which might be employed because of their direct toxic effects on humans, animals and plants...”⁵⁻⁷ The Convention also describes chemical weapons as including not only toxic chemicals but also ammunition and equipment for their disposal. Toxins, produced by living organisms and their synthetic equivalents, are classified as chemical warfare agents if used for military purposes.⁸ Chart 1 gives an overview of some common CWAs.

Chart 1. Some common chemical warfare agents and mimics

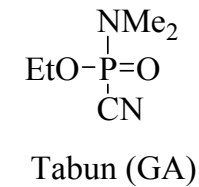
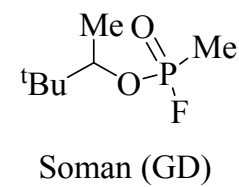
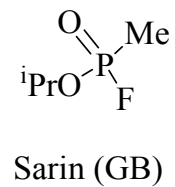
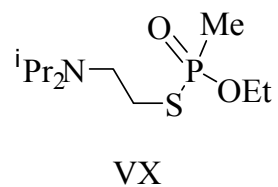
**Mustards
(Sulfur)**



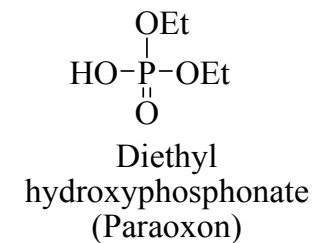
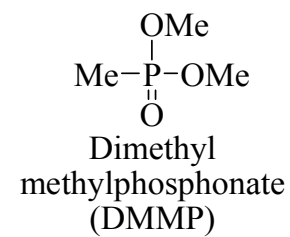
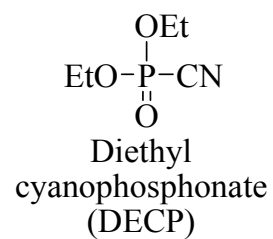
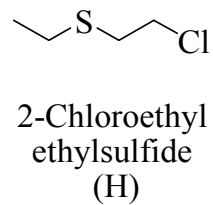
**Mustards
(Nitrogen)**



Nerve Agents



Mimics

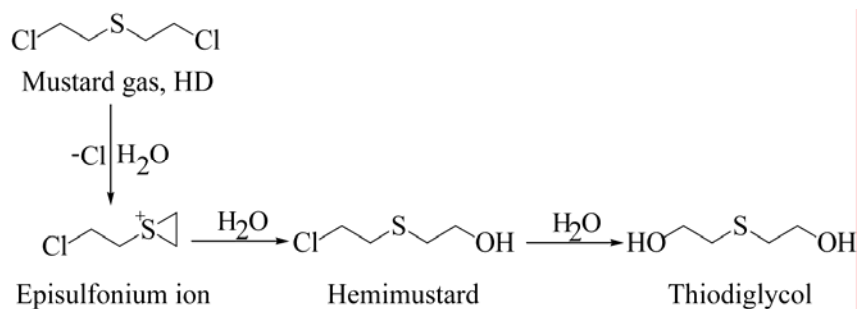


Chemical weapons are classified as weapons of mass destruction by the United Nations. Their production and stockpiling were outlawed by the Chemical Weapons Convention in 1993. Common CWAs can be separated into two major groups of compounds; mustard agents and nerve agents. VX and G-series nerve agents include sarin (GB), soman (GD) and Tabun (GA). The mustard agents are further distinguished by the presence of nitrogen (HN-1, HN-2 and HN-3) or sulfur atom (H, HD and HT) in the compound. For research purposes, mimics are generally used which are less toxic and less reactive than the potent CWA. Chart 1 shows 2-chloroethyl ethylsulfide (H) as a sulphur mustard mimic and diethyl cyanophosphonate (DECP), dimethyl methyl phosphonate (DMMP) and diethyl hydroxyphosphonate (Paraoxon) as nerve agent mimics.

1.2. Chemical Warfare Agents in the Environment

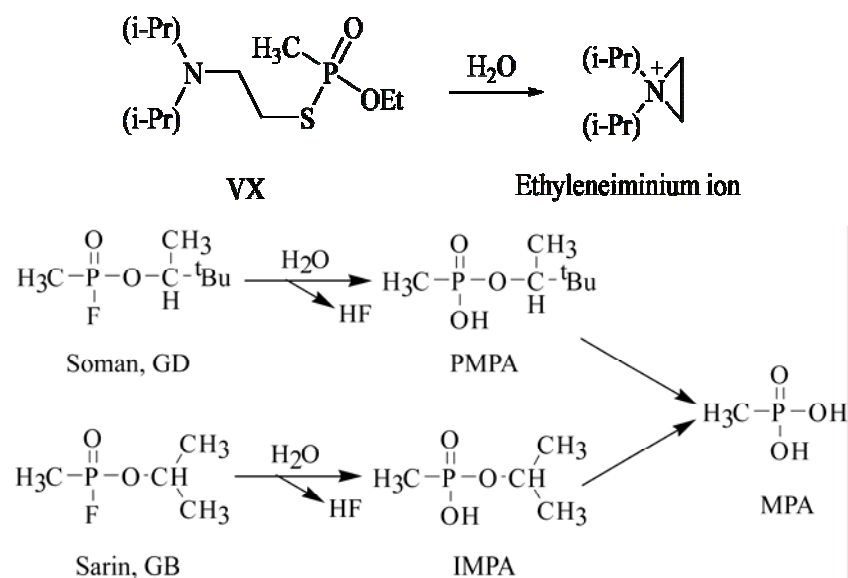
The fate of CWAs in the environment is based on their chemical and physical properties. They often react with water to produce hydrolysis products, which are equally toxic as the CWAs themselves.

Mustard gas: Sulfur mustard is rapidly hydrolyzed. The half-life of dissolved 2-dichloroethyl sulfide, HD ranges from 158 min at 0.6°C to ~ 1.5 min at 40°C and does not vary appreciably in the typical environmental pH range. HD forms an episulfonium ion (Scheme 1.1)⁹ which upon further hydrolysis produces hemimustard and thioglycol. Nitrogen mustards hydrolyze in a more or less similar way and form cationic species (half-lives for HN1, HN2 and HN3 are 12.5 days, 11 hr and 24 hr at 25°C respectively).⁹



Scheme 1.1. Hydrolysis of Sulphur mustard, HD.¹⁰

Nerve agents: Nerve agents are relatively more stable in terms of hydrolysis. The half-life for VX in water at 25°C and pH 7 ranges from 17 days to 42 days and forms an ethyleneiminium ion (Scheme 1.2).^{11,12}



Scheme 1.2: Hydrolysis of nerve agent VX to ethyleneiminium ion^{11,12} and of nerve agents sarin (GB) and soman (GD) to PMPA, IMPA and MPA.¹³

Nerve agents sarin (GB) and soman (GD) produce pinacolyl methylphosphonic acid (PMPA), isopropyl methylphosphonic acid (IMPA) and methyl phosphonic acid (MPA) upon hydrolysis in water (Scheme 1.2).

1.3. Toxicities of CWAs and Their Hydrolysis Products

CWAs and their hydrolysis products are extremely toxic. For example, exposure to mustard gas vapor can result in erythema (capillary congestion, redness of the skin) and gradual vesication (blistering) of the skin. Delayed symptoms of mustard gas exposure are epigastric distress, vomiting, tumorigenic activity and ocular damages, such as conjunctivitis or lacrimation etc.¹⁴ Hydrolysis products of mustard gases also show similar vesicant effects and are lethal in smaller doses. Some of them are found to be carcinogenic.¹⁴

The nerve agents are among the most potent of all chemical warfare agents and are toxic in both liquid and vapor form. They cause nausea, diarrhea, inability to perform simple mental tasks, and respiratory effects which include bronchoconstriction, excess secretion in airways, wheezing, and labored breathing. Exposure to lethal doses, however, causes a person to collapse within seconds and die within 10 minutes after a single deep inhalation. Hydrolysis products of nerve agent, tabun, IMPA, MPA, are found to be skin and eye irritant and the degradation product of sarin is found to affect neuron activity.¹⁰

Table 1.1 summarizes the toxicity data for some common agents and their degradation products.¹⁰ The toxicity of CWAs is measured as an estimate of the dose that can have lethal effects on humans. Lethal Dose₅₀ (LD_{50}) is the estimated dose at which 50% of the population will die if exposed to CWAs. Lethal concentration₅₀ (LC_{50}) and lethal concentration over time₅₀ (LCt_{50}) values represents the concentration of the agent in air and inhalational toxicity of the vapor form of a volatile agent, respectively, necessary to kill 50% of the test subjects. The nerve agent VX is the most toxic of the

common CWAs and very small concentrations are sufficient to achieve detrimental effects – thus it has the lowest LC₅₀ value.

Table 1.1. Toxicity data for some common chemical warfare agents. Given are toxicities of the agents measured by concentration of the agent in air (LC₅₀) and inhalational toxicity (LCt₅₀)¹⁰

Agents	LCt ₅₀ (mg min/m ³)	LC ₅₀ (mg/individual)	LD ₅₀ (mg/Kg)
Tabun (GA)	200	4000	1500
Sarin (GB)	100	1700	1700
Soman (GD)	50	300	350
VX	10	10	10
Mustard (Sulphur, HD)	1500	10000	100
Mustard (Nitrogen, HN-1)	1200	100000	7000
IMPA	---	---	7650
MPA	---	---	5000
Hemimustard	---	---	600
Thiodiglycol	---	---	6610

1.4. Present Detection Technologies

The determination and quantification of CWAs in a precise, convenient and economical fashion is an important goal that has been achieved only partially as these chemicals can be difficult to detect by conventional means.^{7,15-17} The current detection technologies for CWAs can be divided into point and standoff detectors. Point detectors employ techniques such as ion mobility spectrometry, flame photometry, mass spectrometry, photoacoustic infrared spectroscopy, and electrochemistry. Each of these sample the air in the immediate vicinity of the detector.¹⁸ In contrast, standoff detectors use infrared remote sensing technologies from a significant distance. However, the effects of humidity, temperature and composition of the air may influence the detector response and often render false results. Other methods are currently being used but each

has its own limitations. Detection kits that are used for a single measurement are disposable. These are simpler, often cheaper and more sensitive, but cannot be used for continuous monitoring of the air or water quality. At present, the detection limit is restricted to concentrations that are significantly higher than the lethal dose and are fraught with detection ranges and incorrect responses.¹⁸ Chromatographic methods, such as gas and liquid chromatographs, are portable and reliable but are not sensitive enough to detect ultra low concentrations.¹⁸ Biological methods such as immunoassay and inhibition studies, such as monitoring of the acetylcholinesterase activity show great potential for the detection of CWAs but suffer from extensive sample handling procedure and are at present not suitable for real-time monitoring.^{19,20}

1.5. Electrochemical Sensors

Electrochemical detectors have the potential to overcome the shortcomings associated with the present detection technologies. In electrochemical sensors, a working electrode is used to measure the electrochemical response of the system in the form of either potential or current signal. Based on the measured property, electrochemical sensors can be divided into three different categories: conductometric (measuring conductivity change), potentiometric (measuring potential change), and amperometric sensors (measuring current change). Measurements are often carried out in solution in the presence of an analyte by using the electrochemical properties of the CWA or of a chemical reaction that can be detected electrochemically. Electrochemical detectors are potentially sensitive and selective and can be used for continuous monitoring. Electrochemical detectors exhibit a wide linear response, minimal space and

power requirements and are cost efficient. Miniaturization of these devices and compatibility with advanced microfabrication technology make them excellent for on-site monitoring of CWAs. Based on how the electrochemical sensors work, they can be classified into two groups: solution-phase and solid-phase electrochemical sensors.

1.5.1. Solution-Phase Electrochemical Sensors for CWAs

A typical example of solution phase electrochemical sensor involves the electrocatalysis of a nerve agent simulant, diethyl cyanophosphonate (DECP) using an electrochemically generated iodide ion which reacts with DECP (Figure 1.1 (a)).¹⁸ The system shows a positive potential shift at higher concentrations which clearly indicates the presence of DECP. The anodic peak current increases in the cyclic voltammogram (CV) while cathodic peak current decreases as more DECP was added (Figure 1.1 (b)). In this reaction, the electrochemically generated iodine is consumed by the reaction with DECP so that the cathodic peak current is decreased greatly. On the other hand, iodide ion can be bound with DECP, making the oxidation of iodide ion more difficult and the potential of the anodic peak shifts anodically. This method does not allow the detection of DECP in the absence of iodine. Unfortunately, this method has a detection limit of 2×10^{-6} M which represents a minor improvement over common detection systems for CWAs (10^{-5} M) but suffers from interference of atmospheric oxygen.

Nassar *et al.*^{13,21} applied capillary electrophoresis for the identification of nerve agents by conductivity or indirect UV detection. The basic technique is to introduce the sample into the capillary and separate the molecules by applying an electrical field. Samples were introduced to the capillary at a constant pressure (300 mbar) and constant

voltage (-25 and -30 kV for conductivity and UV systems respectively) to control the flow. The shorter migration times were observed at higher fields.

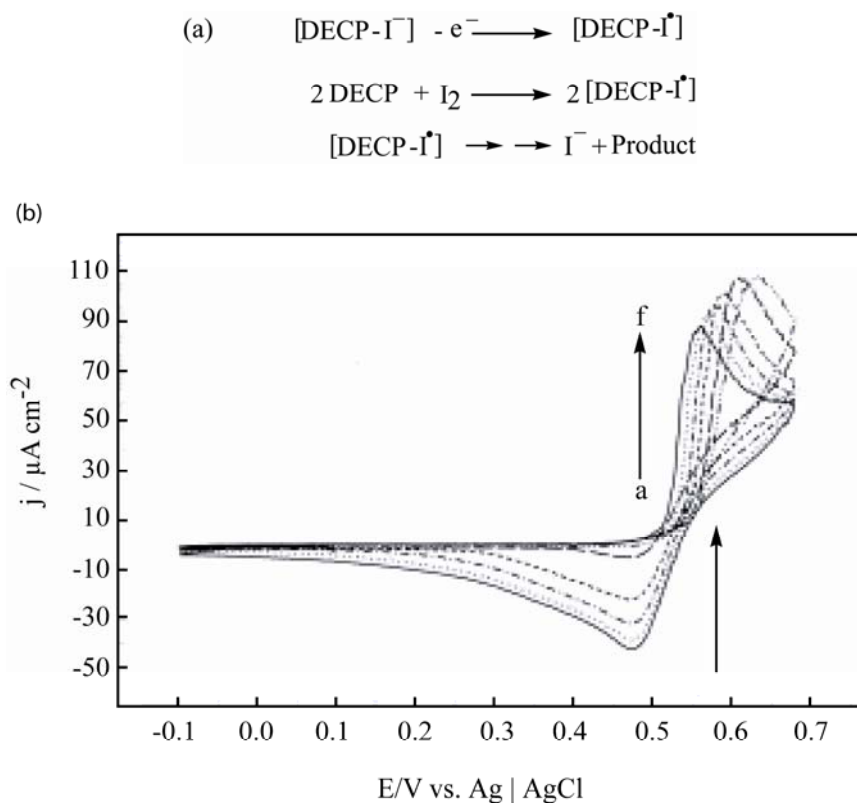


Figure 1.1. (a) Reaction scheme showing electrocatalysis of DECP using electrochemically generated iodide ion. (b) CVs of NaI in the presence of DECP. 0.05 M NaClO₄, 0.05 M phosphate buffer (pH 6.3), 0.40 mM NaI. In (A), DECP (mM): a. 0 (solid curve), b. 0.02, c. 0.05, d. 0.10, e. 0.20, f. 0.30. (Reprinted from Journal of Electroanalytical Chemistry, 466, Xie, Y.; Popov, B. N.; White, R. E., A novel electrochemical method for the detection of nerve gases, 169-176, Copyright (1999), with permission from Elsevier.)

A separation field of -667 V/cm can separate MPA, IMPA, and PMPA within 50 s but for complete separation more time is required. The method provides a good separation efficiency and high sensitivity for the analysis of such compounds. Conductivity measurements give a detection limit of about 75 μg/L, while with UV the detection limit was about 100 μg/L. These developed methods typically achieve complete separations

in less than 3 minutes. A typical run showing the hydrolysis products MPA, IMPA, and PMPA is shown in Figure 1.2.

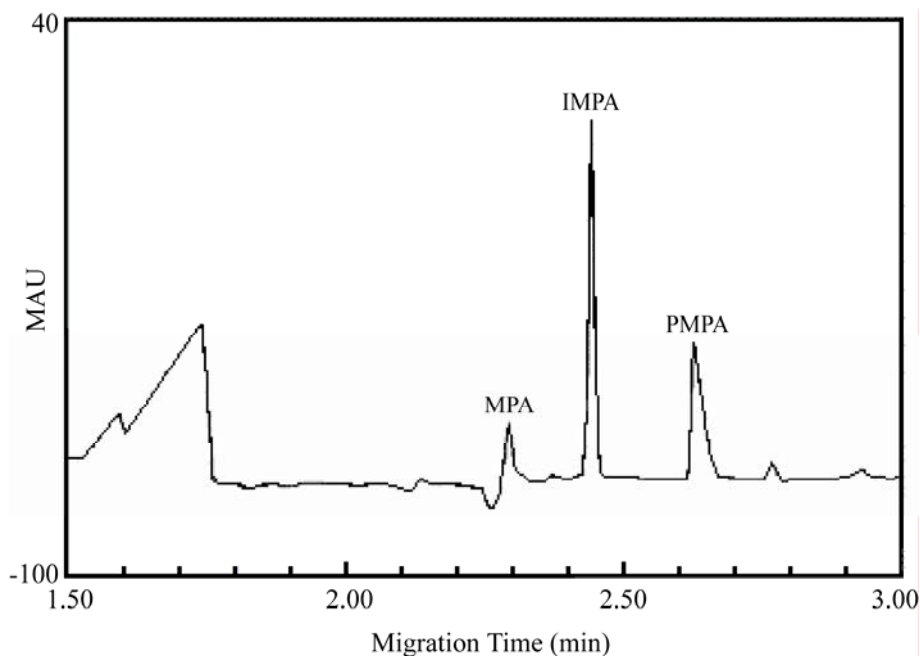


Figure 1.2. Analysis of hydrolysis products of nerve agents MPA, IMPA and PMPA by capillary electrophoresis. pH 4.0; voltage, 30 kV (negative polarity). (Reproduced with permission from *Anal. Chem.* **1998**, *70*, 1085-1091. Copyright 1998 American Chemical Society.)

The same technique was also applied for the detection of VX and the nerve agents Tabun, Sarin and Soman, in environmental samples by Rosso *et al.*²² and by Wang *et al.*^{23,24} Capillary electrophoresis can also be applicable for the screening of nerve agent degradation products MPA, IMPA and PMPA in surface water, groundwater, and soil extracts with a detection limit of around 6 $\mu\text{g/ml}$. These sensors can be used for continuous monitoring but suffers from interference from the acidic gases which dissociate into ions in solution.

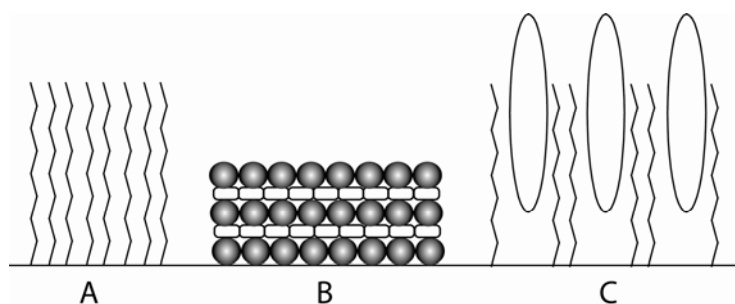
Xie *et al.*^{25,26} proposed a new method for detection of nerve gases Sarin and Soman, on the basis of their catalyzed hydrolysis by metal chelate compounds which shift the potential of the fluoride ion-selective electrode to more positive potential. In his study Xie used diisopropyl fluorophosphates as nerve gas mimics and Cu(II) to bind the hydrolyzed products. It was found that 1:1 Cu(II)–DMBP (4,4'-dimethyl-2,2'-bipyridyl) and 1:2 Cu(II)–TMEDA (*N,N,N',N'*-tetramethylethylenediamine) chelates were the most effective catalysts for accelerating the decomposition of diisopropyl fluorophosphate. Measurement of the variation of open-circuit potential with time was used to detect the hydrolysis products of the nerve agent mimic. A detection limit of 2×10^{-6} M with a potential drop between 40 and 60 mV with a response time of 5 min was achieved.

Hydrolysis products of possible warfare agent trichothecene mycotoxins were detected electrochemically by Freund and co-workers.²⁷ The toxins were hydrolyzed under basic condition at 80°C for 1 hr and then detected by CV and square-wave voltammetry (SWV). The detection limit was found to be 9.1 μ M in solution with a linear response from 0.32 – 32 ppm.

1.5.2. Solid-Phase Electrochemical Sensors for CWAs

While solution-based detection systems rely on a solution phase reaction of the CWA analytes with reactants to generate an electrochemical signal, solid phase sensors rely on electrochemical responses from molecules immobilized on surfaces or their physical interaction with the CWA. The idea behind the development of solid-phase sensors is to overcome some of the problems such as the sensitivity to oxygen encountered in solution-based detection systems. Also, solid state devices can

potentially be miniaturized down to the nanometer level and incorporated into microfluidic devices, which is ideal for the development of portable and inexpensive devices. Scheme 1.3 gives a number of potential approaches ranging from thin films that enable support of enzymatic reactions on surfaces, layer-by-layer assembled materials, and porous patterned materials to detect CWAs. Approach A shows the immobilization of molecules onto a surface. These can be used for the detection of CWAs with or without further modification. Alternatively, layer-by-layer assembly of materials is shown (Scheme 1.3 B). The last material layer bears the active site for detecting CWAs. This often results in an increased sensitivity and selectivity and well suited for enzymatic assays. Lastly, 3-D patterning enables the recognition of specific substrates or agents (Scheme 1.3 C) which can then be detected electrochemically.



Scheme 1.3. Different concepts for designing electrochemical sensors based on self-assembly. (A) self-assembly, (B) layer by layer assembly and (C) channel formation by molecular imprinting

Enzymatic reactions are very promising since they offer high selectivity. An example is an amperometric sensor based on a surface-immobilized organophosphorus hydrolase (OPH) enzyme.^{19,28} In this approach, the sensor relies on the anodic detection of enzymatically hydrolyzed products at the top OPH layer on a sulfonated

tetrafluorethylene co-polymer layer. OPH hydrolyzed the organophosphorus pesticides, paraoxon to *p*-nitrophenol which went through electrooxidation (Figure 1.3 (i)) and on successive increments chronoamperometric measurement showed an increase in current depending on the concentration of paraoxon (Figure 1.3 (ii)). Well-defined current signals were observed for these micromolar increments in the substrate concentration. The resulting calibration plots (inset of Figure 1.3 (ii)) display high sensitivity for paraoxon (slope = 1.67 nA / μ M). The detection limit was found to be 20 nM.¹⁹

This idea of using OPH enzyme is also integrated into a single-channel microchip for fast screening of nerve agents.²³ The sensor uses a chip-based flow injection approach coupled with separation modules for convenient distinction between total and individual nerve agents. The assay rates are 360 and 30 per hour for total screening and individual measurements, respectively. This reaction method is also applied to the formation or use of nanomaterials onto the surfaces to get a fast response for nerve agents like VX.^{29,30} The hydrolytic activity of enzymes is used to produce nanoparticles on the surface which generate an electrochemical signal for detecting various nerve agents.

Shulga *et al.*³¹ used electro-polymerization of pyrrole for the entrapment of the biocatalyst pyrroloquinoline quinone to produce a sensor to detect thiol-containing degradation products of VX based on the amperometric measurement at 0.38 V. The sensor has a detection limit in the 3.0-4.5 μ M range.

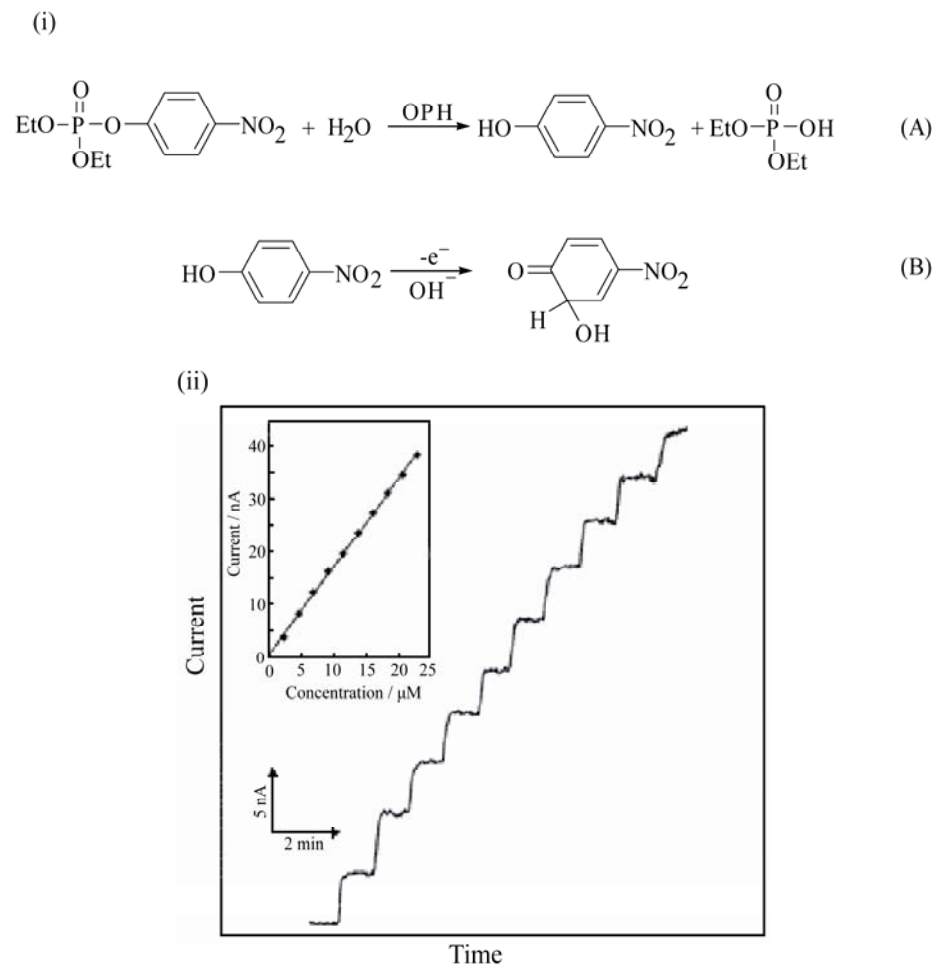


Figure 1.3. (i) Reaction scheme of OPH-catalyzed hydrolysis of organophosphate nerve agent (A) followed by electrooxidation of the liberated *p*-nitrophenol (B). (ii) Current-time amperometric response to successive increments of organophosphorus pesticides paraoxon. Insets: calibration plots for paraoxon. (Reproduced with permission from *Anal. Chem.* **1999**, *71*, 2246-2249. Copyright 1999 American Chemical Society.)

Layer-by-layer assembly onto self-assembled carbon nanotubes combined with an enzymatic approach provided a platform for the detection of nerve agents and organophosphorus pesticides.²⁰ Acetylcholinesterase (AChE) is immobilized onto the negatively charged nanotube surface to make a sandwich-like structure followed by alternative deposition of the cationic polymer, poly(diallyldimethylammonium chloride) (PDDA) and AChE as shown in Figure 1.4. Carbon nanotubes act as a transducer and

the polymer used in this case provides a micro-environment suitable for native AChE activity.

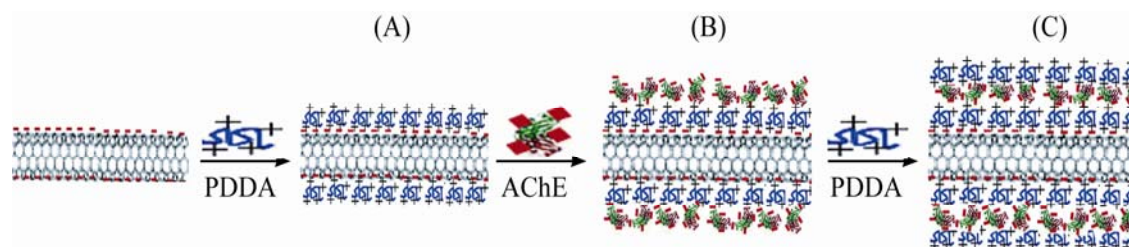
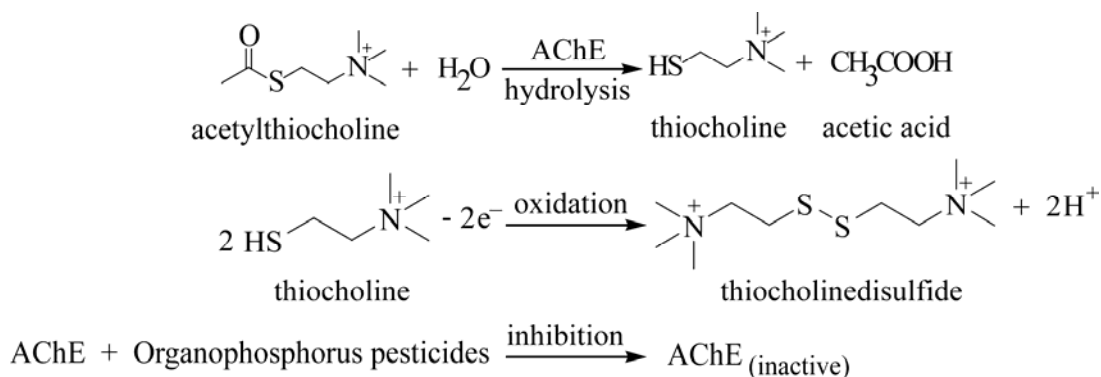


Figure 1.4. Schematics of layer-by-layer electrostatic self-assembly of AChE onto carbon nanotube: (A) assembling positively charged PDDA on negatively charged nanotube; (B) assembling negatively charged AChE; (C) assembling the second PDDA layer. (Reproduced with permission from *Anal. Chem.* **2006**, 78, 835-843. Copyright 2006 American Chemical Society.)

In this system AChE was used to catalyze the hydrolysis of acetylthiocholine (the substrate used to modulate the AChE activity by organophosphorus pesticides) to thiocholine which could be further oxidized to thiocholinedisulfide at constant potential at the nanotube to generate an oxidative current (Scheme 1.4). It was found that the current increased rapidly with the increase of concentration of acetylthiocholine. Organophosphorus pesticides inhibited this hydrolytic activity of AChE enzyme by making it inactive (Scheme 1.4) and the inhibition was monitored by measuring the oxidation current produced by thiocholine at the nanotube (Figure 1.5 (a)). The % inhibition was calculated from the current response and plotted against the concentration of the nerve agents (Figure 1.5 (b)). Under the optimal conditions, the detection limit was found to be as low as 0.4 pM with a 6-min response time.



Scheme 1.4. Reaction scheme of enzymatic sensor using AChE as enzyme for detecting organophosphorus pesticides.²⁰

A similar approach was used by Joshi *et al.*³² using multi-wall carbon nanotubes without a flow injection system. In this system, immobilized AChE showed a similar response by using the same method for the same pesticide with a detection limit of 0.5 nM.

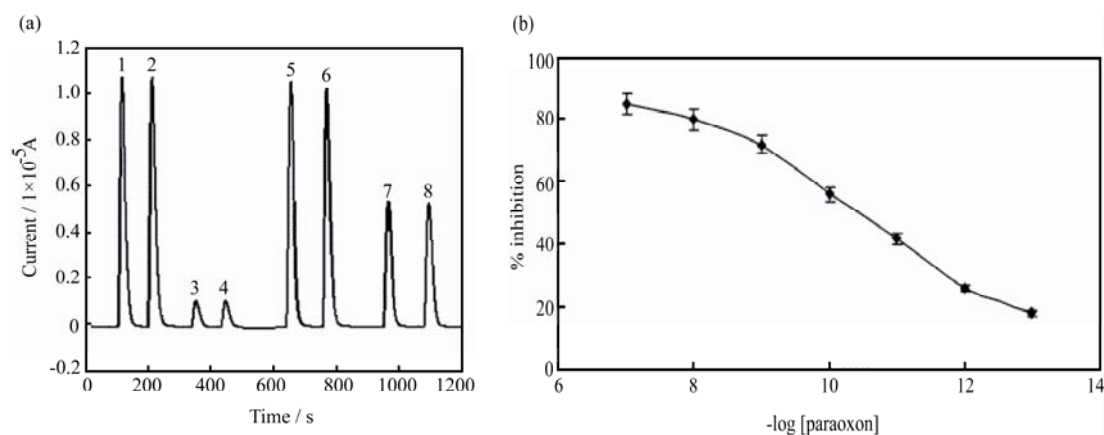
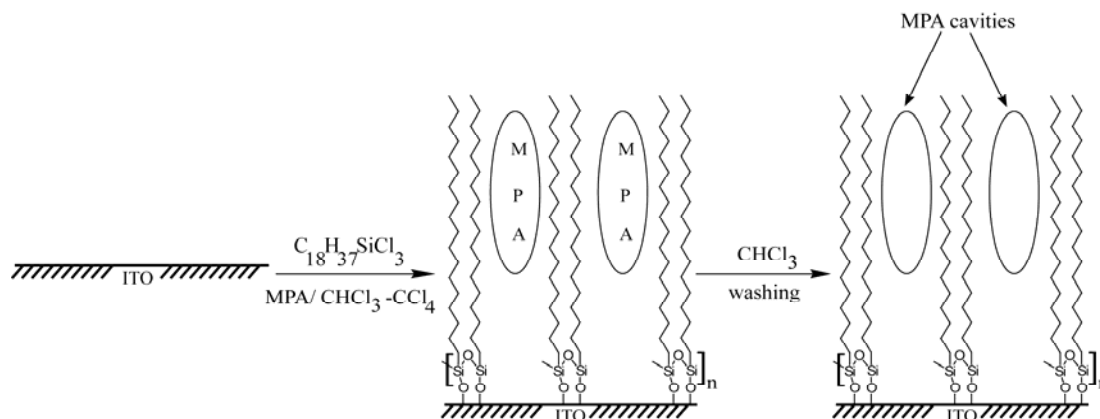


Figure 1.5. (a) Typical amperometric responses of PDDA/AChE/PDDA/nanotube/glassy carbon biosensor during the flow injection analysis of organophosphorus pesticide, paraoxon. Signals 1 and 2, initial enzyme activity; signals 3 and 4, after incubating 6 min with 0.1 nM paraoxon; signals 5 and 6, after regeneration; signals 7 and 8, after incubating 6 min with 10 nM paraoxon. (b) Inhibition curve of the PDDA/AChE/PDDA/nanotube/glassy carbon biosensor to different concentrations of paraoxon. (Reproduced with permission from *Anal. Chem.* **2006**, *78*, 835-843. Copyright 2006 American Chemical Society.)

Layer-by-layer assembly was also used to immobilize OPH enzyme on the pH sensitive Al/p-Si/SiO₂ layer which on exposure to organophosphorus pesticides showed an increase in capacitance.³³ This change in capacitance was plotted against the concentration of nerve agents to construct the calibration curve for the sensor. Layer by layer assembly was also utilized by Lei *et al.*³⁴ to immobilize a microbe, *Pseudomonas putida*, on the cell surface which will express OPH to detect *p*-nitrophenyl substituted organophosphate nerve agents. Surface-expressed OPH catalyzed the transformation of *p*-nitrophenyl substituted organophosphate nerve agents to *p*-nitrophenol, which was subsequently degraded by the microbe. A carbon paste electrode was used for the electrochemical measurements.

Detectors for nerve agents simulants by measuring resistance were reported by Hopkins *et al.*³⁵ An array of carbon black/organic polymer composite was used which change resistance upon exposure of nerve agents. The detection limit is in the range 47 – 240 µg/m³ for nerve agent degradation products DMMP. The sensor did not suffer from interferences with water and organic solvents, such as methanol and toluene. Fabrication of channels was achieved by a surface imprinting technique on indium tin oxide (ITO) surfaces for potentiometric measurements of the nerve gas hydrolysis product MPA.³⁶ ITO is electrically conducting and provides an ideal surface for the formation of a siloxane film. Zhou *et al.*³⁶ was able to form a thin film of octadecylsiloxane on ITO in the presence of MPA. The MPA was then washed away, leaving channels presumably shaped like MPA (Scheme 1.5). The resulted sensor demonstrated higher complementary steric and functional adsorption ability to the template molecule than that of the untemplated surface.



Scheme 1.5. Formation of selective MPA cavities on ITO-coated glass plates by molecular imprinting. (Redrawn from reference 36.)

The result of this approach was a system that allowed the potentiometric detection of MPA down to a detection limit of 5×10^{-5} M and even selectivity for this material. The system recognized MPA and the potential changed slowly at the initial concentration (50 μ M) and then rose rapidly as more MPA was added (Figure 1.6).

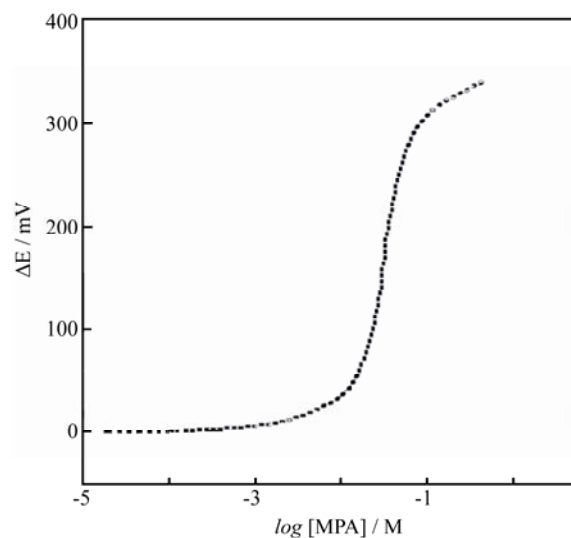
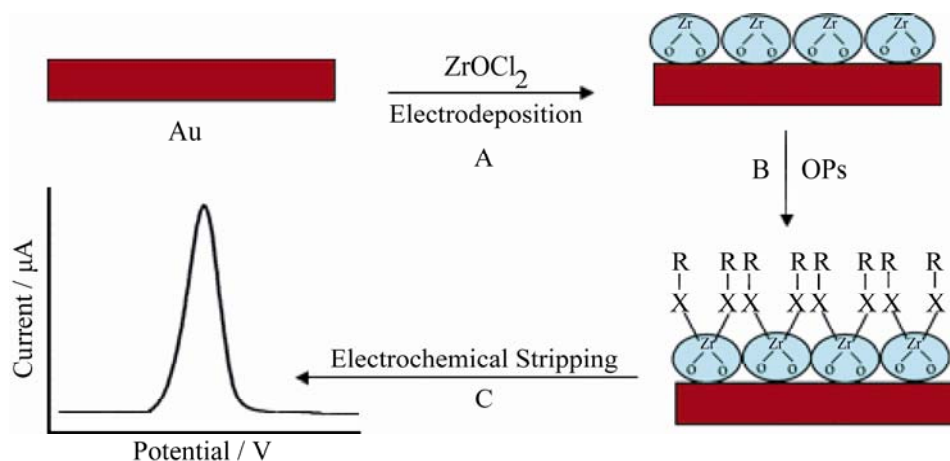


Figure 1.6. Potentiometric responses of the MPA cavity sensor for MPA. $[\text{MPA}](\text{CHCl}_3/\text{CCl}_4) = 2.5 \times 10^{-2}$ M; $[\text{octadecyltrichlorosilane}] = 8.0 \times 10^{-4}$ M. Adsorption time 3 min. (Reproduced with permission from *Anal. Chem.* **2004**, *76*, 2689-2693. Copyright 2004 American Chemical Society.)

Liu *et al.*³⁷ used zirconia nanoparticles as selective sorbents for CWAs on metal substrates and detected CWAs by electrochemical measurement techniques. Zirconia electrochemically formed a layer over the gold substrate. Because of the strong affinity of zirconia for the phosphoric group nitroaromatic organophosphates, it strongly binds with the zirconia nanoparticle surface (Scheme 1.6). SWV was used to quantify the amount of organophosphate pesticides bound and demonstrated the ability to detect the CWAs. The response was linear over a range of 5 – 100 ppb with a lowest detection limit of 1 ppb. A lower detection limit of 13 ppb was achieved with a carbon paste electrode as the transducer surface.



Scheme 1.6. Scheme of electrochemical sensing of nitroaromatic organophosphorus pesticides. (A) Electrodeposition of zirconia nanoparticle to gold electrode surface; (B) nitroaromatic organophosphorus pesticides adsorb to zirconia nanoparticle surface; (C) electrochemical stripping detection of nitroaromatic organophosphorus pesticides; X = O or S and R = nitroaromatic organophosphorus pesticide group. (Reproduced with permission from *Anal. Chem.* **2005**, *77*, 5894-5901. Copyright 2005 American Chemical Society.)

The sensors discussed in this section are simple and can be used for rapid and direct detection of CWAs. However, there are factors that can be improved such as

detection limits, selectivity and reproducibility. Also, in case of enzyme sensors, OPH are not commercially available which limit the use of this material for preparing sensors. AChE based sensors suffer from poor selectivity, irreversible response or a multi-step protocol (involving a substrate addition and incubation).¹⁹ Sensors based on electrochemical responses of redox active molecules immobilized on metal surfaces could be a potential method to overcome these drawbacks as the molecules could orient themselves in a particular fashion to achieve selectivity with lower detection limit.

At present, electrochemical sensors are based largely on enzymatic assays (See Figure 1.3 and 1.4). No direct method exists that detects changes in the redox response of a chemically modifiable label. The research outlined in this thesis focuses on this aspect and aims to fill the current knowledge gap.

1.6. Objectives and Research Proposal

The objective of this research is to develop a sensor that gives a reproducible electrochemical response to CWA mimics.

I propose to address this problem by using redox active molecules that can undergo a reaction with CWAs and their mimics. Receptor molecules have been developed in which one group is attached to a particular substrate and will allow sensing of cations, anions and neutral molecules electrochemically.^{38,39} Of these receptors, ferrocene (Fc) complexes have recently received much attention because of their unique structural and electronic properties.⁴⁰⁻⁴⁵ The Fc group can be attached to amide and urea moieties for electrochemical sensing of anions.⁴⁴ Fc substituted macrocycles such as

cyclams, cryptands, aza-crowns, crown ethers and calixarenes were shown to sense alkaline-, alkaline earth-, transition-metals and lanthanide ions.^{42,45-47}

I have selected Fc conjugates that carry an amino group directly attached to one of the cyclopentadienyl rings. These molecules are ideal for this purpose, since they are stable in the reduced and oxidized form and can be readily modified to improve specificity. The amino Fc-derivatives will exhibit interesting donor capabilities which can be utilized to detect electrophilic cationic species which include hydrolysis products of CWAs.⁴⁸ Complexation of a neutral or ionic species generally occurs at the recognition site, which causes an electrochemical response of the Fc group detectable by CV.

Chapter 2 will show the reactivity of an aminoferrocene derivative with CWA simulants in solution. This is followed by Chapter 3, presenting the results on surface-supported aminoferrocenes for the detection of CWA mimics.

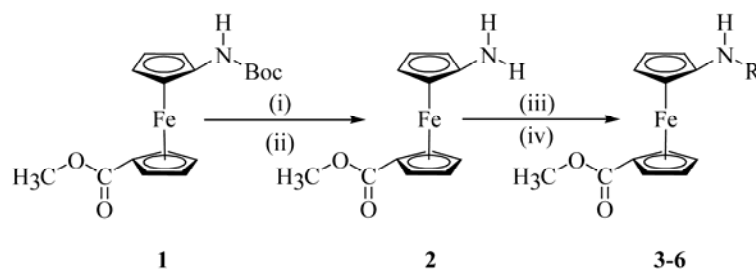
Chapter 2. Reactions of Aminoferrocene with Chemical Warfare Agent Mimics:

Solution Study

In this chapter, the basic chemistry of 1-amino-*n'*-ferrocenemethylcarboxylate, 1,*n'*-H₂N-Fc-COOCH₃ (**2**) toward alkylating agents is explored. It is expected that the reaction with alkylating reagents, such as EtSCH₂CH₂Cl and (CN)(EtO)₂P(O) will lead to well-defined organometallic products. In all cases, the *N*-substitution is expected to significantly affect the redox properties of the ferrocene group. Thus, as part of this study, the effect of the substitution on the electrochemical properties of the redox group is evaluated and the observed changes are rationalized by molecular orbital calculations.

2.1. Synthesis and Characterization

Boc-deprotection of Boc-NH-Fc-COOMe (**1**), by trifluoroacetic acid in dichloromethane solution under inert conditions results in the formation of 1-amino-*n'*-ferrocenemethylcarboxylate, 1,*n'*-H₂N-Fc-COOMe (**2**). Alkylation reactions of the amino group of compound **2** are summarized in Scheme 2.1. Alkylations with MeI and EtI readily resulted in formation of the corresponding 1,*n'*-MeHN-Fc-COOMe (**3**) and 1,*n'*-EtNH-Fc-COOMe (**4**), while the reaction with ClCH₂CH₂Set, MA, a simulant for the mustard gas HD, gave the expected 1,*n'*-EtSCH₂CH₂HN-Fc-COOMe (**5**). Reaction with diethylcyanophosphonate (CN)(EtO)₂P(O), NA, a simulant for the nerve agent tabun resulted in the formation of 1,*n'*-(EtO)₂P(O)NH-Fc-COOMe (**6**). Purification of these materials was achieved by column chromatography, giving red oils, which were further analyzed spectroscopically.



Scheme 2.1. Reactions of **2** with alkylating agents: (i) TFA in DCM, (ii) Et₃N, (iii) EtOH and (iv) saturated NaHCO₃; **3**: R = Me, **4**: R = Et, **5**: R = CH₂CH₂SEt, **6**: R = (P=O)(OEt)₂.

All of the compounds exhibited a weak absorption band in the visible region with a $\lambda_{\text{max}} \geq 451$ nm, typical of the d-d transition in ferrocene derivatives.⁴⁹ The IR spectrum of these compounds show a typical C=O band close to 1700 cm⁻¹ and all N-H stretching bands are below 3400 cm⁻¹ (Table 2.1) which indicates that N-H bonds in these compounds are hydrogen bonded.⁵⁰⁻⁵² The ¹H and ¹³C{¹H}-NMR spectra of compounds **3-5** were recorded in CDCl₃ while compound **6** was recorded in MeOD because of its limited solubility in CDCl₃. The ¹H and ¹³C{¹H}-NMR spectra of compounds **3-6** exhibit signals that are closely related to those observed for related 1,*n*'-diaminoferrocene analogues [Fe(η-C₅H₄CH(CH₂)₄NMe)₂]⁵³ (**7**), [Fe(η-C₅H₄(CH₂)₂NMe₂)₂]⁵³ (**8**) and the Fc-urea dimethyl-1',1'-ureylenedi(1-ferrocenecarboxylate)⁵⁴ (**9**). The ¹H-NMR spectra of compounds **3-5** exhibited the expected 1:1:1:1 pattern for the Cp protons of the 1,*n*'-disubstituted ferrocene group, with chemical shifts in the range of δ 3.87–4.81.

Due to the tendency of compound **6** to decompose, NMR studies were carried under Schlenk conditions in dilute solutions. Compound **6** exhibits a single resonance in

the ^{31}P NMR at δ 48.7 (vs external 85% H_3PO_4). It is suggested that in compound **6** the downfield shift may be due to the extended delocalization of the π -electron systems of the Fc moiety and the phosphonate. In order to clarify this point, we carried out DFT calculations (B3LYP, vide infra). The HOMO of compound **6** is shown in Fig. 2.

Table 2.1. Selective spectroscopic data for compounds **3–6** (**3–5** in CDCl_3 , **6** in MeOD)

	3	4	5	6
IR (KBr, cm^{-1})	3375 (N-H), 1712 (C=O)	3360 (N-H), 1700 (C=O)	3340 (N-H), 1708 (C=O)	3245 (N-H), 1720 (C=O)
^1H -NMR (δ/ppm)	3.81 (s, 1H, N- H), 3.80 (s, 3H, COOMe)	3.81 (s, 3H, COOMe), 3.79 (s, 1H, N-H)	3.81 (s, 1H, N- H), 3.80 (s, 3H, COOMe)	3.21 (s, ester CH ₃), 1.14 (q, CH ₂ -2H), 0.80 (t, CH ₃ -3H)
^{13}C -NMR (δ/ppm)	173.0 (C=O), 51.7 (COOCH ₃)	171.8 (C=O), 65.5 (COOCH ₃)	159.0 (C=O), 51.4 (COOCH ₃)	171.9 (C=O), 19.8 (COOCH ₃)
Mass Spec.	Calc. 273.0452 Expt. 273.0453	Calc. 287.0608 Expt. 287.0610	Calc. 347.0642 Expt. 347.0637	Calc. 395.0584 Expt. 395.0574
Yield (%)	8	25	10	8

Atkinson *et al.*⁵⁵ also observed a ^{31}P NMR signal due to the phosphorus in the P=O bond attached to Ph_2 at δ 33.2. A similar peak is observed at δ 29.5 for O=P–N in $[\text{Cl}(\text{Me}-\text{P}=\text{O})(\text{N}=\text{P}-\text{Ph})(\text{Me})(\text{OCH}_2\text{CF}_3)]$ (**10**) by Neilson and coworkers⁵⁶ where phosphorus is attached to the highly electron withdrawing chlorine atom and electron releasing methyl group. In the ^{13}C -NMR spectrum the peak corresponding to the carbon in C=O moiety for compounds **2–6** appears at δ 172.

2.2. Electrochemical Study

Since one of the objectives of this study was to evaluate the effects of N-substitution on the redox properties of the Fc group, we decided to carry out electrochemical studies using CV. As would be expected, $E_{1/2}$ is sensitive to the substituent.⁵⁷ CVs for the free amine **2** and the phosphonate **6** are shown in Figure 2.1 and a summary of the results for all compounds is provided in Table 2.2.

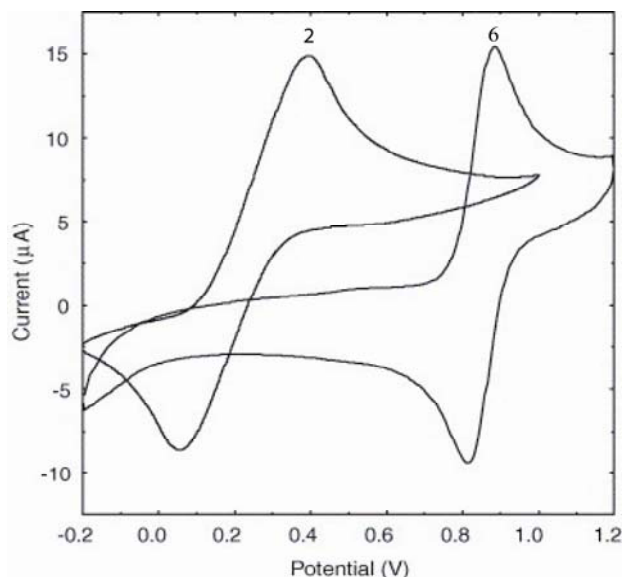


Figure 2.1. Cyclic voltammetry of compounds **2** and **6** in CH₃CN solution with glassy carbon electrode as working electrode, Pt wire as counter electrode and Ag/AgCl as reference electrode and 0.2 M tetrabutylammonium perchlorate (TBAP) as supporting electrolyte with a scan rate of 100 mV/s. Concentration of the compounds: 1 mM

All compounds exhibited a quasi-reversible one-electron oxidation with peak current ratios close to unity. The halfwave potentials ($E_{1/2}$) for all the compounds were observed in a range from 215 to 850 mV versus Ag/AgCl with anodic to cathodic peak

separation (ΔE) in the range of 62–88 mV. While the observed $E_{1/2}$ values for the alkyl-substituted amino systems **3–5** are cathodically shifted with respect to the free amine, indicating that these systems are easier to oxidize, the Boc-protected amine **1** and the aminophosphonate **6** are anodically shifted, making it more difficult to oxidize the Fc group in these systems. The electron donating alkyl groups facilitates the oxidation process due to the higher electron density at iron and results in a cathodic shift of the oxidation potential. This shift is expected to be higher for the Et and CH₂CH₂SEt derivatives **4** and **5**. However, their $E_{1/2}$ is slightly anodically shifted compared to the methylated system **3**.

Figure 2.1 shows that substitution of the free amine **2** for an aminophosphonate in **6** results in a significant anodic shift of 588 (± 7) mV. Amino group in **2** donates additional electron density into the ferrocene core and facilitating its oxidation. But in **6**, due to the electron withdrawing effect of the substituent, the ferrocene core is less electron rich making it more difficult to oxidize and oxidation occur at higher potential. In order to rationalize our observations, it was decided to carry out additional calculations.

Table 2.2. CV parameters for compounds **2–6** (solvent: CH₃CN, scan rate: 100 mV/s, working electrode: glassy carbon, reference electrode: Ag/AgCl, counter electrode: Pt wire, electrolyte: 0.2 M TBAP)

Compound	$E^{1/2}$ (mV)	ΔE (mV)	i_{pa}/i_{pc}
1	489 (7)	114 (5)	0.99
2	262 (6)	88 (3)	1.00
3	215 (5)	62 (2)	1.09
4	234 (4)	82 (2)	1.01
5	233 (6)	82 (3)	0.90
6	850 (8)	70 (4)	1.02

2.3. Quantum Mechanical Calculations

The geometries of compounds **2–6** were optimized using the DFT routine provided in GAUSSIAN-03 (B3LYP using a 6-31G basis set). The calculation clearly shows that due to lower charge on ferrocene of compound **3** compare to that of compound **2**, it will be easy to oxidize but in compound **4**, the Fc group has more charge which results in a more positive redox potential. In compound **3** conjugation of the methyl group can occur while in compound **4** the methyl group cannot take part in conjugation through saturated $-\text{CH}_2$ bridge.

A similar effect was observed by Hocek *et al.* where the electron withdrawing effect of a conjugated alkyne bridge enabled electronic coupling to the Fc which was responsible for the higher redox potential.⁵⁸ But in compound **6** the aminophosphate group anodically shifts $E_{1/2}$ of the Fc group. Theoretical considerations suggest that this is due to the electron withdrawing effect and π -acceptor properties of the phosphate group. This can be seen more clearly from Figure 2.2, which shows the HOMOs of compounds **2–6**.

The HOMO of compound **6** is highly stabilized due to orbital interactions between the Fc and the aminophosphate. It is highly stabilized compared to compounds **2–5**. In addition, the shape of the orbital at the aminophosphate group is different than those of other compounds. While in compounds **2–5** the π -conjugation within the Cp ring is intact with little extension over the substituents, a new orbital node is present in compound **6** facilitating electronic delocalization into the substituent.

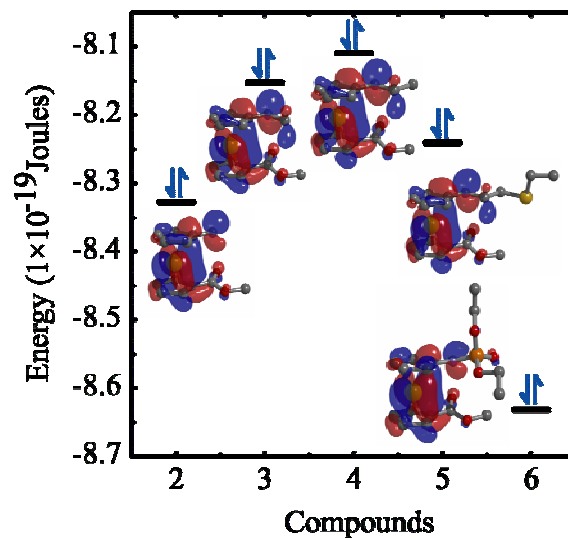


Figure 2.2. HOMO contours and energies of compounds 2–6.

In this chapter synthesis and characterization of fully protected ferrocene amino acid, [Boc-NH-Fc-COOMe] (**1**) is reported. This compound reacts with CWAs mimics to give a series of well-defined chemical products that were also fully characterized spectroscopically. Importantly, their electrochemical properties in solution are significantly different and characteristic to the specific class of CWA mimic.

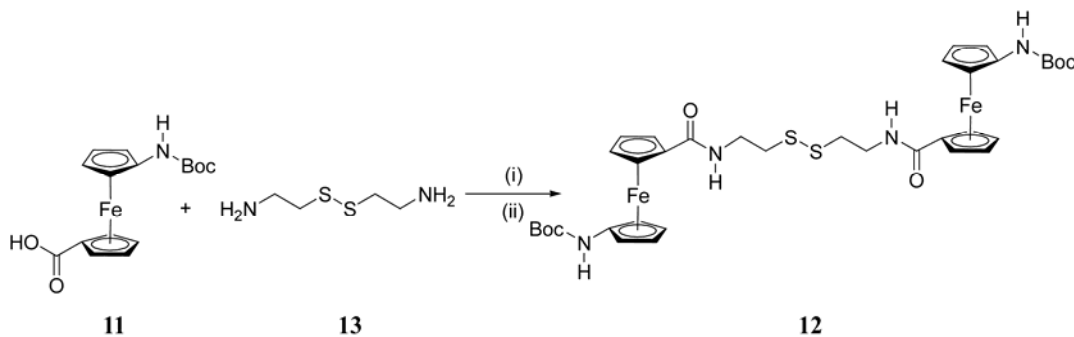
With the success in solution study, we further modified the amino ferrocene derivative by reacting with cystamine so that we can immobilize the sensor material onto gold surface to get a robust sensor platform. This assembly of molecules on the surface will also allow us to have a miniaturized device which eventually can lead us to a portable device.

Chapter 3. Surface Studies of Amino Ferrocene Derivatives on Gold: Towards Electrochemical Sensors for Chemical Warfare Agents

In this chapter, we report the synthesis and characterization of the cystamine conjugate of ferrocene amino acid [BocHN-Fc-CO-CSA]₂. This molecule is equipped with an amino group that directly linked to the redox receptor. We speculated that the redox potential of the Fc group would be strongly affected by the reaction of the amino group with alkylating agents on surface, which may eventually lend itself to the electrochemical detection of alkylating agents. For this purpose, we prepared thin films of [BocHN-Fc-CO-CSA]₂ on gold and carried out surface reactions with simulants for chemical warfare agents, such as EtSCH₂CH₂Cl (MA), a simulant for sulfur mustards HD and (CN)(EtO)₂P(O) (NA), a simulant for nerve agents Tabun. Their reaction with the surface-bound ferrocene derivative results in the formation of N-substituted products. The surfaces are probed using a series of spectroscopic and electrochemical techniques, including x-ray photoelectron spectroscopy, ellipsometry and quartz crystal microbalance.

3.1. Synthesis and Characterization

The orange-red ferrocene amino acid conjugate, [(BocNH)Fc(CO)CSA]₂, (**12**) was synthesized using the EDC/HOBt protocol⁵⁹ starting from the Boc-protected aminoferrocene carboxylic acid, BocHN-Fc-COOH (**11**) and cystamine, NH₂CH₂CH₂SCH₂CH₂NH₂, (**13**) as shown in Scheme 3.1.



Scheme 3.1. Synthesis of compound [(BocNH)Fc(CO)CSA]₂ (**12**). (i) CH₂Cl₂, HOBt, EDC; (ii) Et₃N.

The symmetrical disulfide was fully characterized spectroscopically. The compound exhibit absorption band in the visible region with a $\lambda_{\text{max}} = 442$ nm, typical of the d–d transition in ferrocene derivatives.⁴⁹ In the ¹H-NMR spectrum, compound **12** exhibits two resonances at δ 7.27 and at δ 6.39, assigned to the CSA amide and the Fc-carbamide group, respectively (Figure 3.1 (a)). These two groups also give distinct signals in the ¹³C-NMR at δ 171.3 for the amide C=O group and at δ 154.3 for the Fc-carbamide group (Figure 3.1 (b)). The chemical shift of amide groups in Fc-conjugates is sensitive to H-bonding and shifts downfield of δ 7.00 indicate the involvement of amide NHs in H-bonding.^{50,60} This is supported by the presence of an Amide A resonance at 3334 cm⁻¹ in infrared spectroscopy, indicating H-bonding.^{20,61-68} The chemical shifts of the inequivalent Cp protons of the Fc group are comparable with reported shifts and are observed as four distinct singlets in the region of δ 4.72 – 4.05. These chemical shifts are comparable to those of other di-substituted Fc-systems, like [(AcNHC₅H₄)Fe(C₅H₄CONHMe)]⁶⁸ (**14**) and [(AcNHC₅H₄)Fe(C₅H₄CON(Cy)CONHCy)] (Cy = cyclohexyl) (**15**).⁶⁷

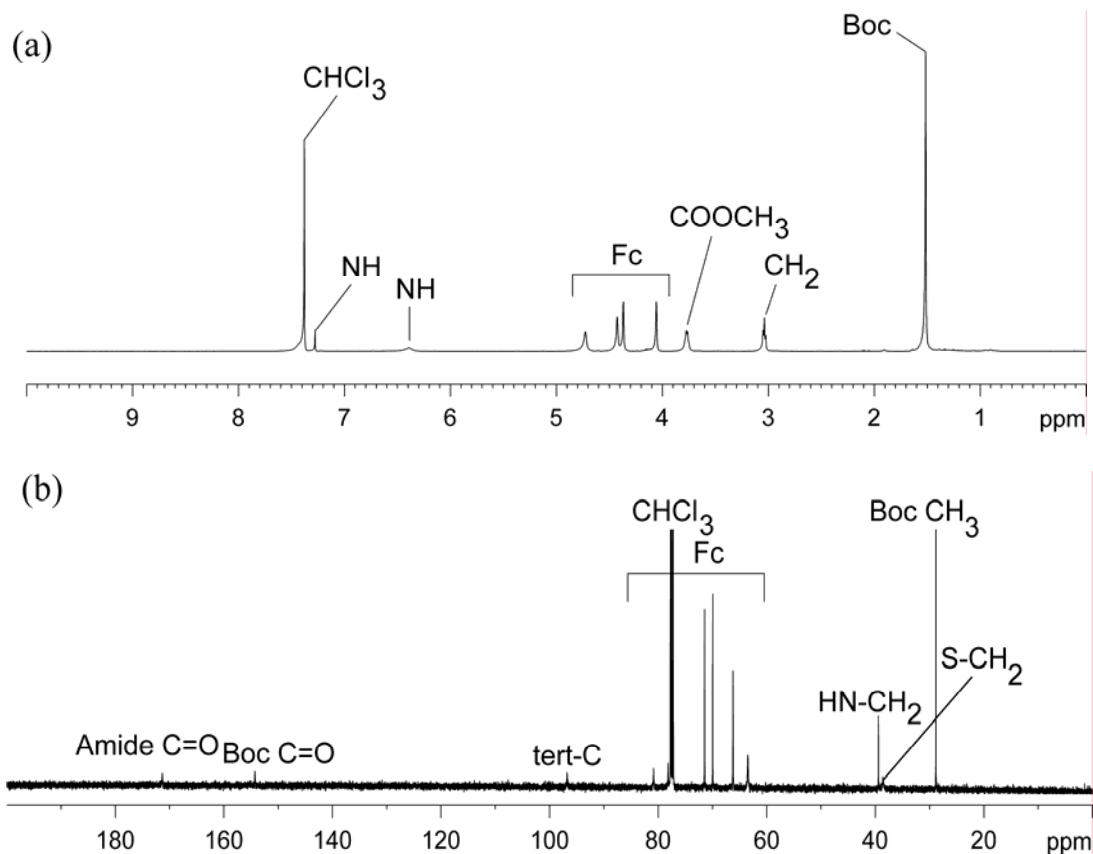


Figure 3.1. (a) ^1H -NMR spectrum of $[(\text{BocNH})\text{Fc}(\text{CO})\text{CSA}]_2$ (**12**) and (b) ^{13}C -NMR spectrum of $[(\text{BocNH})\text{Fc}(\text{CO})\text{CSA}]_2$ (**12**) in CDCl_3 .

The ORTEP structure of compound **12** is shown in Figure 3.2 (a). Selected bond distances and angles for compound **12** are given in Table 3.1. The Cp rings are almost parallel to each other in both ferrocene molecules [$1.0(2)^\circ$ and $1.9(4)^\circ$, respectively]. The substituted groups are slightly twisted out of plane of the Cp rings to which they are attached (twist angles (β) are 24.71° (0.16) and 8.20° (0.30) respectively for Cp planes and amide planes on two ferrocenes through Fe1 and Fe2). The conformation of Fc1 can be described as 1,5' with respect to the orientation of the substituents (Figure 3.2 (b)), while that of Fc2 can be described as approximately 1,1' (Figure 3.2 (c)).

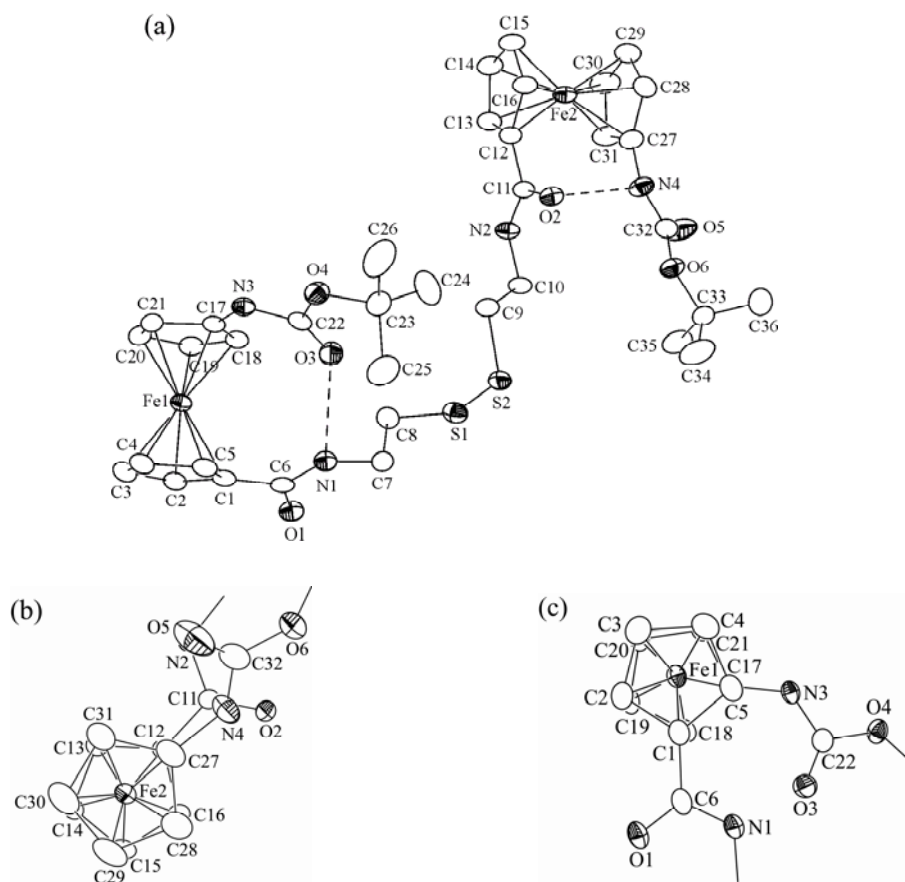


Figure 3.2. (a) ORTEP plot of $[\text{BocNH}(\text{C}_5\text{H}_4)\text{Fe}(\text{C}_5\text{H}_4)\text{C}(\text{O})\text{NHCH}_2\text{CH}_2\text{S}]_2$ (**12**) shown at the 30% probability level. (b) 1,5' conformation of Fc1 (c) 1,1' conformation of Fc2 with respect to the orientation of the substituents. H-atoms are omitted for clarity.

These conformations are stabilized by intramolecular H-bonding between N1 and O3 and N4 and O2. The intramolecular $\text{N}(\text{H})\cdots\text{O}=\text{C}$ distances are 2.849(3) Å and 2.989(3) Å, respectively, indicating fairly strong hydrogen bonding.⁶⁰ This is in line with the NMR and IR measurements which also indicate the presence of H-bonding in solution and the solid state. In addition, individual molecules of **12** are strongly interconnected through intermolecular H-bonding between carbonyl oxygen [O(1) and O(2)] of the amide and amino hydrogen [N(2)(H), N(3)(H)] forming an effective H-

bonded network in the crystalline state with H-bonding distances of 2.789(3) and 2.795(3) Å (Table 3.2).

Table 3.1. Selected bond distances (in Å) and bond angles (in °) for compound **12**

Bond	Distance	Bond	Distance
C1-C6	1.467(4)	C12-C11	1.470(4)
C6-O1	1.240(3)	C11-O2	1.253(3)
C17-N3	1.415(4)	C27-N4	1.419(4)
N3-C22	1.342(4)	N4-C32	1.348(4)
C22-O3	1.213(4)	C32-O5	1.200(4)
S1-S2	2.037(13)		

	Angle		Angle
C1-C6-N1	116.9(2)	C12-C11-N2	117.9(2)
C12-C11-O2	120.7(2)	C27-N4-C32	122.9(3)
C1-C6-O1	121.8(3)	N3-C22-O3	126.0(3)
Cg1-Fe-Cg2	179.2(5)	Cg3-Fe-Cg4	179.3(5)

θ angles

Fc1 1.0(2) Fc2 1.9(4)

Twist angles (β)

Fc1 24.71(0.16) Fc2 8.20(0.30)

Torsion angles (ω)

Fc1 -75.28(0.25) Fc2 -9.34(0.25)

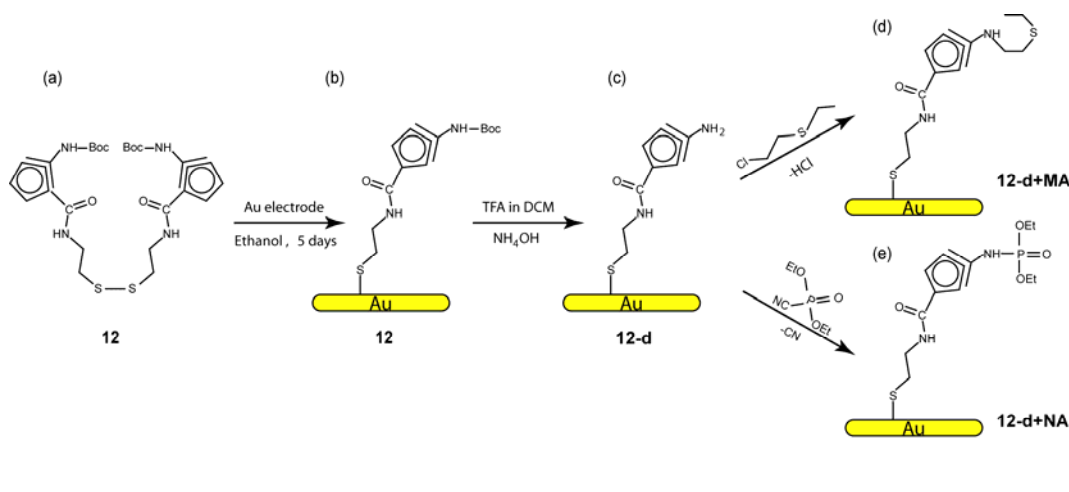
Table 3.2. D(H)⋯A distances (in Å) for compound **12**

D(H)⋯A	d(D⋯A)
N1H⋯O3	2.849(3)
O3⋯N1H	2.849(3)
N4H⋯O2	2.989(3)
O2⋯N4H	2.989(3)
N2H⋯O1	2.789(3)
O1⋯N2H	2.789(3)
N3H⋯O2	2.795(3)
O2⋯N3H	2.795(3)

3.2. Surface Studies

3.2.1. Cyclic Voltammetry

Compound **12** is equipped with a disulfide group, which allows the formation of films on gold surfaces. Our general approach of making monolayer is shown in Scheme 3.2. Deprotection of the Boc-group in films of compound **12** by TFA results in the formation of a film having free amine group (**12-d**).



Scheme 3.2. Schematic view of surface modifications of compound **8** (a) in solution (b) on surface (c) deprotection of **12** to **12-d** (d) exposure of **12-d** with 1 ppm MA, **12-d+MA** and (e) exposure of **12-d** with 1 ppm NA, **12-d+NA**.

A typical CV of the film before and after deprotection of compound **12** is shown in Figure 3.3 (a). The formal potential of a film of **12** was observed at $E^0 = 317(15)$ mV versus Ag/AgCl with a peak separation of the cathodic and anodic peaks of $\Delta E_p = 52(6)$ mV and a peak current ratio close to unity. A lower peak current ratio in case of **12-d+MA** indicates a more irreversible system with a different forward and backward electron transfer rate. Based on the integrated Faradaic signal, we obtained a surface concentration Γ for compound **12** of $\Gamma = 1.08 \times 10^{-10}$ (3.48×10^{-11}) mol/cm² with a

footprint of 130(51) Å²/molecule while from crystallographic data the molecular area of **12** was found to be 36 Å²/molecule. The difference may be due to the tilt angle or disrupting of hydrogen-bonding of two adjacent cyclopentadienyl rings which will allow the movement of the substrate and eventually will occupy more space. Similar results were also observed for the other amino ferrocene systems.⁶¹

After deprotection, the film of **12-d**, the formal potential E^0 experiences a cathodic shift to 262(10) mV vs Ag/AgCl, while the reversibility of the process is not affected. Surface concentration (Γ) changes to 3.17×10^{-11} (5.80×10^{-12}) mol/cm² which indicates a 29% loss of the material compared to a film of compound **12**. We assume that some of the weakly bound surface molecules which arise due to the differences in adsorption energies of the adsorption sites on the heterogeneous surface desorbed during the deprotection process or some of the Au-S bonds are protonated by TFA and subsequently come off the surface.^{61,69} Typical CVs for a film of **12-d** after exposure to MA and NA are shown in Figure 3.3 (b).

The ΔE_p values indicate that **12**, **12-d** and **12-d+NA** undergo reversible while **12-d+MA** undergoes a quasi-reversible redox process (i_{pa}/i_{pc} values are close to unity except **12-d+MA**). The ΔE_{fwhm} values are significantly larger than the ideal values (97 mV) for minimal lateral interaction which indicate that the electroactive centers on the surface are non-interacting.⁷⁰⁻⁷² A footprint of 130(51) Å²/molecule of **12** on the surface also support that. We assume that different orientations of molecules may generate a very disordered surface. Also presence of different chemical environment from the intact and broken H-bond between the adjacent amide groups of the same molecule may give rise to phase-separated domains which cause the observed peak broadening. During

the scanning process in cyclic voltammetry a particular domain may have slightly different response from its adjacent domain due to the different surface charges associated with redox centers. This may cause fluctuation in the potential and give rise to broad peaks.⁷⁰⁻⁷³

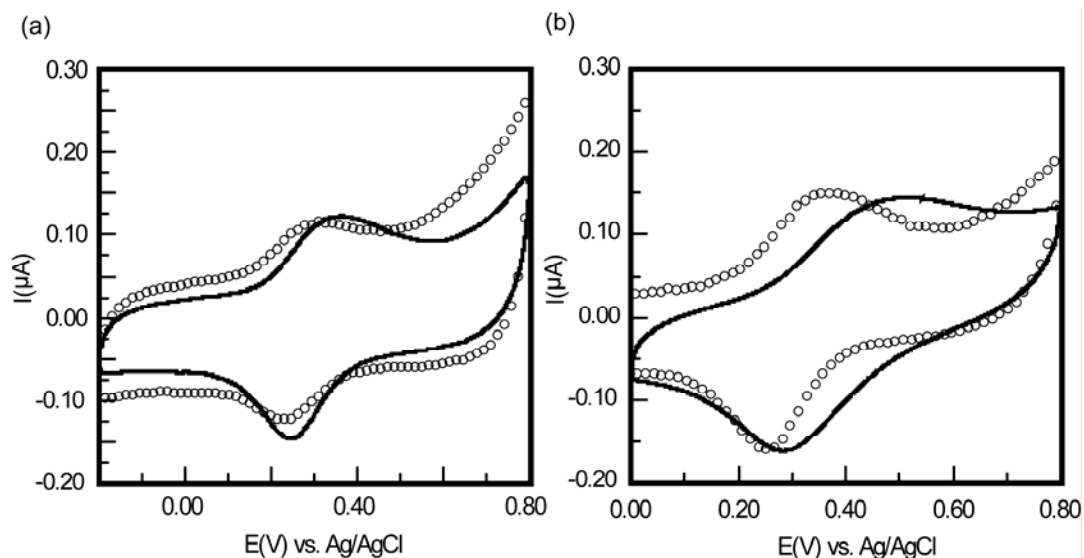


Figure 3.3. (a) CVs of 25 μm gold microelectrode surfaces modified with **12** (solid line) and deprotected **12-d** (\circ). (b) **12-d** after exposure to 1 ppm MA, (**12-d+MA**) (\circ) and NA, **12-d+NA** (solid line) in 2.0 M NaClO_4 solution. Scan rate 100 V/s, reference electrode Ag/AgCl (3M KCl) and counter electrode Pt wire.

We tried to improve the peak sharpening by using butanethiol diluted surface of **12** but without any apparent success. Dilution after deprotection results in losing the electrochemical signal in CV which may be due to alkylation and desorption of the molecule.^{74,75} We assume deprotection process etches the surface and makes it more vulnerable to thiol molecules.

3.2.2. Differential Pulse Voltammetry

DPV were taken for all systems (Figure 3.4) to resolve the issue of peak broadening. Figure 3.4 (a) and (b) show the DPVs of compound **12**, **12-d** and **12-d+MA** and **12-d+NA**.

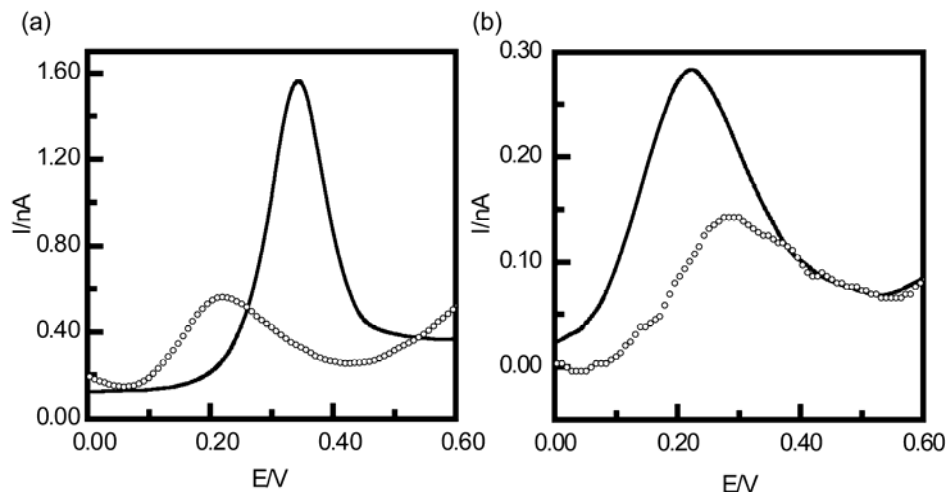


Figure 3.4. (a) DPVs of 25 μm gold microelectrode surfaces modified with **12** (solid line) and deprotected **12-d** (\circ). (b) **12-d** after exposure to 1 ppm MA, (**12-d+MA**) (solid line) and NA, **12-d+NA** (\circ) in 2.0 M NaClO_4 solution. Amplitude: 0.05 V, pulse width: 0.05 sec and pulse period: 0.2 sec.

The peak broadening in DPV is assumed to be due to highly disordered surface resulting from deprotection of Boc-group on **12**. Also the decrease in peak current supports our assumption of alkylation and desorption of surface molecules by MA and NA. The film thicknesses of the surfaces in Figure 3.3 were measured by ellipsometry and all values shown in Table 3.3, lie close to the values calculated for molecular dimensions of the compounds by **Spartan 2.0** software.

Table 3.3. Electrochemical parameters and thicknesses of **12** on 25 μm gold electrodes and Au on Si substrates

Surfaces	E° (mV)	ΔE_p (mV)	i_{pa}/i_{pc}	ΔE_{fwhm} (mV) (oxidation peak)	Film Thickness (\AA)	Calc. Film Thickness
12	317 (± 15)	52 (± 6)	1.10	190 (± 10)	12 (± 2)	9 ^a
12-d	262 (± 10)	50 (± 5)	1.01	180 (± 10)	6 (± 1)	9 ^b
12-d+MA	310 (± 5)	110 (± 3)	0.71	222 (± 15)	10 (± 4)	16 ^b
12-d+NA	314 (± 3)	59 (± 2)	0.93	145 (± 12)	7 (± 2)	15 ^b

^aCalculated from crystal; ^bCalculated from **Spartan 2.0**

3.2.3. Surface Titration

The variation of formal potentials with the logarithm of concentration of MA and NA are shown in Figure 3.5 and indicate a response over a wide concentration range of for two of the CWA mimics tested.

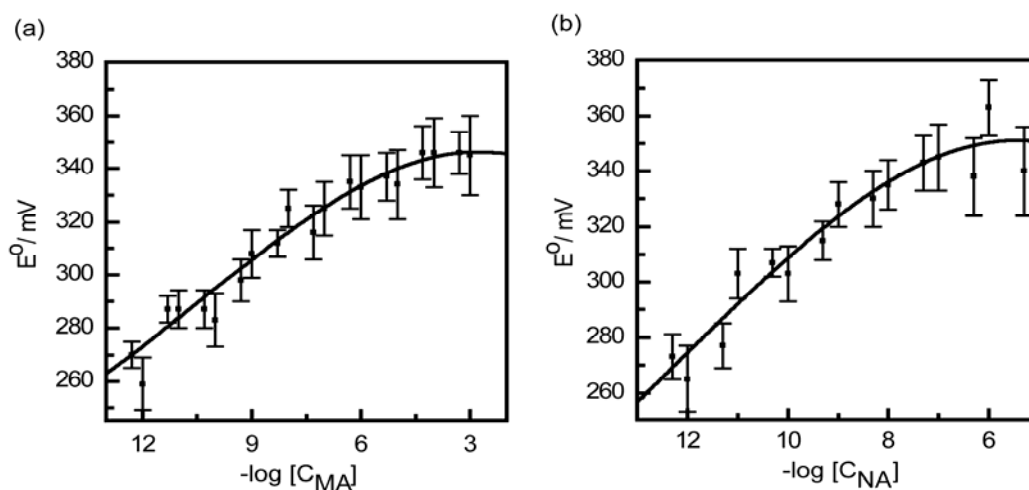


Figure 3.5. (a) Changes in potential on addition of increasing concentration of MA and (b) NA to surface immobilized **12-d**. Working electrode: gold microelectrode (25 μm diameter); reference electrode: Ag/AgCl; counter electrode: Pt wire; electrolyte: 2M NaClO₄; scan rate: 100V/s.

In each case, formal potentials move toward more positive values as the concentration of MA and NA increases. Best fit line of the data in Figure 3.5 (a) shows that for the mustard mimic the formal potential increase upon addition of MA but then levels off at high concentrations, most likely due to a saturation of the sensor surface. In case of NA, the behavior is similar, but saturation is already reached after the addition of 1 ppm of NA (Figure 3.5 (b)). We assume that with this higher concentration, the molecule on the surface is alkylated by the analytes and then stripped off. These observations are in agreement with our observations in our solution study. Extended surface studies clearly show the formation of the expected chemical species on the surface.

3.2.4. Quartz Crystal Microbalance

In order to get more insight into the chemistry that takes place on the surface involving the ferrocene amino acid cystamine conjugate, we decided to carry out a study involving an electrochemical quartz crystal microbalance and determine changes in mass that take place upon the deprotection of **12** and its subsequent reactions with MA and NA. For this purpose, a gold covered silicon crystal (9 mm diameter, AT-cut, CH Instruments) was exposed to an ethanolic solution of compound **12** in a procedure identical to that described for the films prepared on gold electrodes. Changes in the resonance frequency Δf were monitored as a function of time (in sec).

Figure 3.6 shows a plot of the changes in resonance frequency Δf in Hz versus time for a film **12** before and after Boc-deprotection. In the absence of TFA, the film of **12** is stable and no changes in Δf were observed. However, upon addition of a solution of TFA (40% in CH_2Cl_2), rapid loss of CO_2 and isobutene cause an increase in Δf of

2.42 Hz, which corresponds to a net mass loss of 3.39 ng. This mass change is higher than the calculated mass change based on the surface coverage of **12** with a footprint of 130(51) Å²/molecule which can be rationalized by desorption of molecules by the deprotection process.

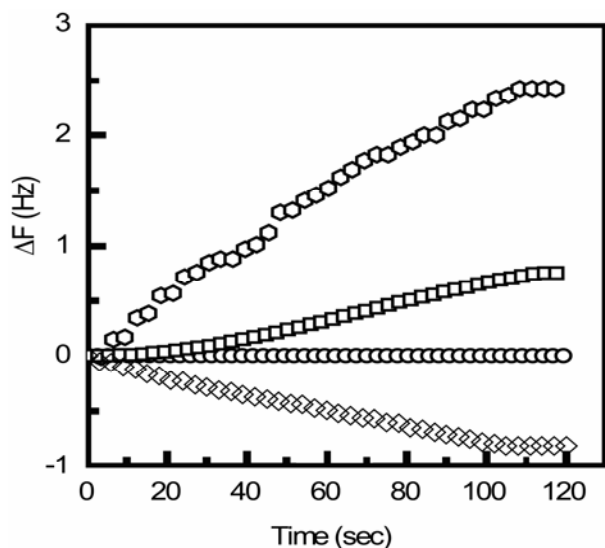


Figure 3.6. Typical QCM plot for frequency changes (Δf) vs. time of the Au surfaces on quartz crystal modified with **12** (○), deprotected **12-d** (◐), **12-d+MA** (◑) and **12-d+NA** (◒) at 25 °C.

A mass gain of 2.3 (± 0.3) ng is achieved when MA is added to **12-d** on the surface. We attribute this change to the reaction between the free amine **12-d** and the ion formed by hydrolysis of MA. The mass change is higher than the expected value (2.17 ng for 83% reaction as calculated from XPS data). We assume that the increased mass is due to the adsorption of MA itself on the surface by physisorption or chemisorption via formation of an Au-S bond. When NA is added (ion mass: 137.09) the frequency drops still further ($\Delta f = -0.81$ Hz) which indicates a mass gain (4.5 (± 0.5) ng) on the quartz crystal. The excess mass gained by reaction with NA may be due to binding of NA with

surface species via H-bonding.⁶² Similar trends with EQCM experiments were also observed by other researchers.⁷⁶⁻⁷⁹ The mass and frequency changes are given in the Table 3.4.

Table 3.4. Frequency and mass changes on QCM after deprotection and exposure of **12-d** to MA and NA

Surfaces	Frequency (f) Hz	Frequency change (Δf) Hz	Mass change (Δm) ng	Calc. mass changes (ng)
12	0.00	-	-	-
12-d	2.42	2.42	3.4 (± 0.4)	2.46
12-d+MA	0.75	1.67	2.3 (± 0.3)*	2.17
12-d+NA	-0.81	3.23	4.5 (± 0.5)**	2.82

*mass gain from **12-d** to **12-d+MA**, **mass gain from **12-d** to **12-d+NA**

3.2.5. X-ray Photoelectron Spectroscopy

Film compositions of the surfaces were also measured by XPS to investigate the reactions that occurred from the deprotection and addition processes. Deconvolution of the XPS S_{2p} (Figure 3.7 (a)) gives rise to a doublet at 161.8 (S 2p_{3/2}) and 163.0 eV (S 2p_{1/2}) with a 2:1 area ratio and a peak separation of 1.2 eV. The binding energy of the S 2p photoelectrons at 161.8 eV is a conformity of thiolate sulfur bonded to the Au surface via Au-S bond.⁸⁰⁻⁸⁷ Figure 3.8 (c) and d show two peaks with a XPS binding energy of 707.8 and 715.7 eV which are the characteristic signatures of the Fe(II) and Fe (III) (2p) respectively of a ferrocene group.^{34,88} This unambiguously confirms that **12** is attached to the surface. Figure 3.7 (b) shows deconvolution of the S 2p peak after the reaction of **12** with MA.

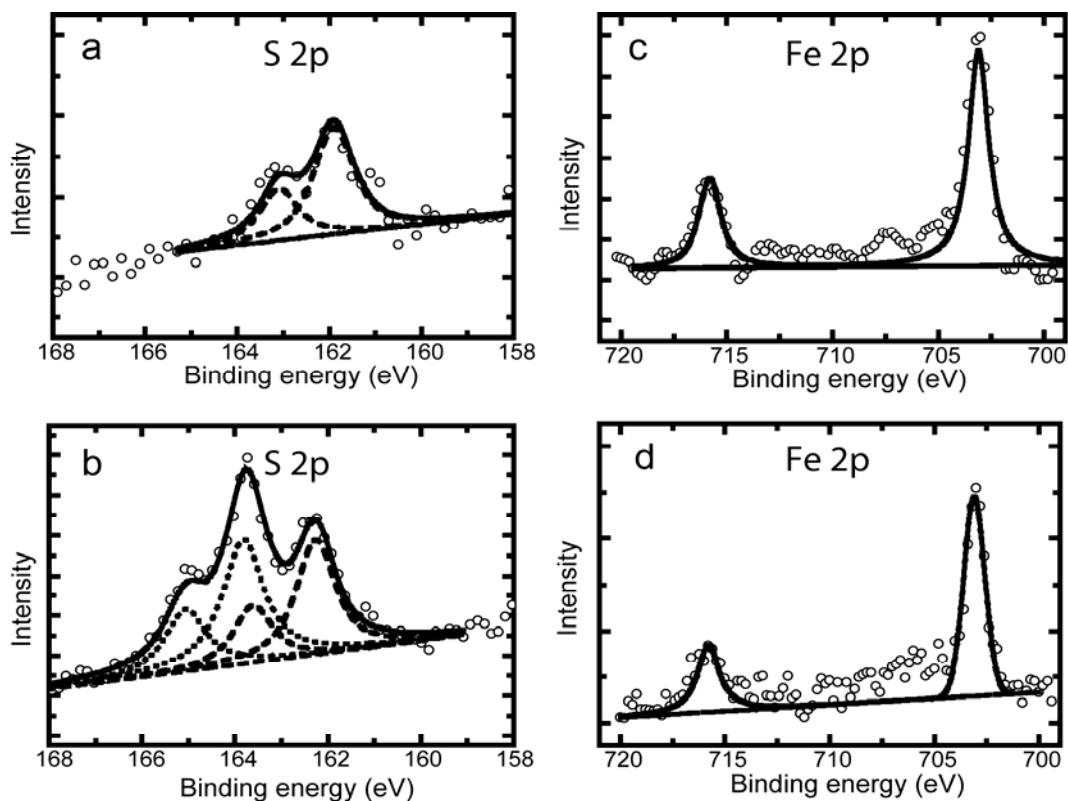


Figure 3.7. XPS S 2p spectra for (a) **12** (b) **12-d+MA** and Fe 2p spectra for (c) **12** and (d) **12-d+NA** films on gold surface.

Surface bounded sulfur shows peaks at 162.2 and 163.6 eV as in the case of **12** whereas the peaks at 163.8 and 165.0 eV are assigned to the reacted sulfur species from MA which is not bounded to Au surface.^{80,81,83-85} The area ratio of the two types of sulfur was found to be 1.2:1 which indicates a 83% yield compared to 70% of that of **12-d** with NA under identical conditions.

The more convincing evidence comes from N1s spectra which show clearly that **12-d** reacts with MA and NA. As shown in Figure 3.8 (a) for **12**, the N1s spectra exhibit two distinct peaks at 399.3 and 399.9 eV with full width at half maximum (fwhm) of 1.15 eV. The peak at 399.9 eV is attributed to CSA amide, N-C=O species, whereas the peak at 399.3 eV is most likely due to N-atom of carbamide.^{34,89} The peak area ratio of

1:1 is consistent with the presence of two distinct nitrogen environments in **12**. The N1s binding energy for CSA amide, N–C=O at 399.9 eV is identical for **12** and **12-d** and in case of **12-d+MA** and **12-d+NA** it shifts 0.2 and 0.1 eV to positive value respectively.

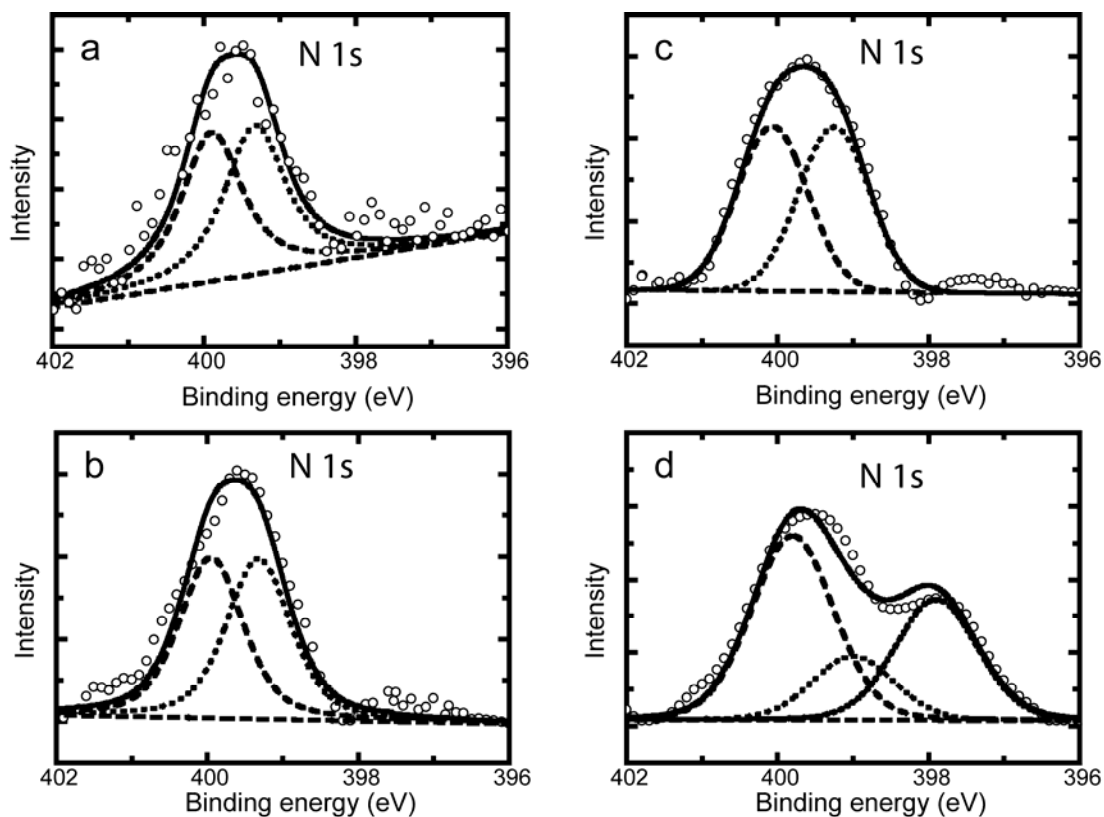


Figure 3.8. XPS N1s spectra for (a) **12** (b) **12-d** (c) **12-d+MA** (d) **12-d+NA** films on gold surface.

On the other hand, the carbamide nitrogen on conversion to free amine gives an identical peak at 399.2 eV which shifts to 399.1 eV in case of **12-d+MA**. This nitrogen is strongly affected by the reaction with NA bond and shifts to 397.8 eV while at the same time some residual free amine shows at 399.3 eV. We assume that electrons become more delocalized over the ferrocene ring to the oxygen atom attached with phosphorus through P–N bond due to the electron withdrawing effect and π -acceptor

properties of the phosphonate group. This gives the nitrogen atom more electron density which in case of MA is less pronounced because of the saturated alkane bridge.

Table 3.5. N1s binding energies for **12** and modified films

Modified surfaces	N1s (eV)		Ratio of peak area
	Carbamide-N	CSA amide, N-C=O	
12	399.3	399.9	1:1
12-d	399.2	399.9	1:1
12-d+MA	399.1	400.1	1:1
12-d+NA	397.8, 399.3	400.0	(0.7:0.3):1

The peak area ratio of this carbamide nitrogen and residual free amine was found to be 0.7:0.3. This also supports that only 70% of the free amine was reacted in case of addition of nerve agent mimic on to the surface. The change in N1s binding energy is summarized in Table 3.5. All other elements C1s, O1s and Au_{4f} give their characteristic peak at the usual positions.

4. Conclusions and Future Research

4.1. Conclusions

The reaction of 1-amino-*n'*-ferrocenemethylcarboxylate, 1,*n'*-H₂N-Fc-COOMe (**2**), with electrophiles was studied. *N*-Alkylations of **2** result in the expected products, while the reaction with diethylcyanophosphonate results in the formation of the corresponding aminophosphonate derivative. The solution electrochemistry of these compounds showed a significant shift in the halfwave potential which was rationalized by quantum mechanical calculations. This result holds promise for the development of a sensor based on the redox chemistry of aminoferrocene.

The cystamine conjugate, [BocNHFcCOCSA]₂, was immobilized onto gold and was used for the detection of chemical warfare mimics. Cyclic voltammetry studies of the surface bound molecules showed a similar shift in the halfwave potential in the presence of CWA mimics. XPS showed that chemical reaction occurred between the CWA mimics and the free amine group of compound **12** results in the formation of chemically well-defined species. Titration experiments with CWA mimics gave a detection limit of 0.1 ppb.

4.2. Future Research

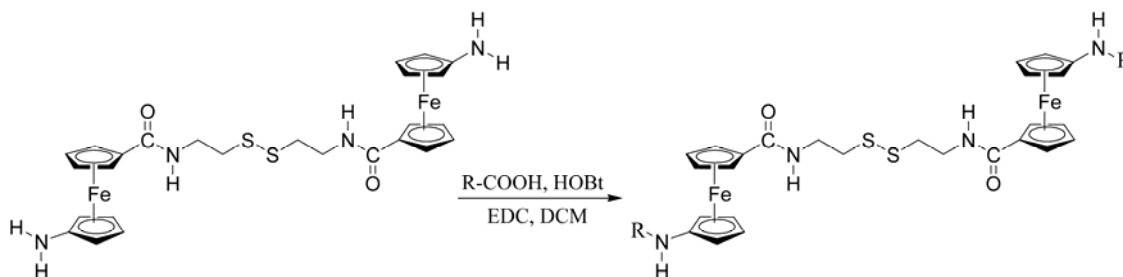
A series of critical investigations need to be carried out addressing issues related to possible environmental effects and interferences.

The response of the film of compound **12** as a function of temperature needs to be evaluated. In addition, it is important to determine if additives such as metal ions, solvents or even dirt, will interfere the results.

At present, the system investigated in this thesis is not selective. Other ferrocene based systems need to be developed to address issues related to selectivity. Besides these, there are more questions remain unanswered:

1. Can this system selectively detect mustard gases and nerve agents?
2. Can the sensitivity of the present system be further increased?
3. Can the system differentiate among different CWA mimics belonging to the same class?
4. Can the incubation time be shortened?
5. Can this system be used for continuous monitoring?

Some of the questions may be answered by modifying our sensor compound **12** using amino acid modified aminoferrocene derivatives.



Scheme 4.1. Scheme for modification of present sensor compound. R = Boc-His, Boc-Trp, Boc-Asp, Boc-Glu, Boc-Gln, Boc-Asn and Boc-Cys.

Amino acids, for example, histidine,^{16,90,91} glutamic acid,^{16,90,92} cysteine,¹⁶ aspartic acid,⁹² tryptophan,^{16,90} glutamine,⁹² and asparagine⁹² were shown to have exclusive reactivity towards CWAs in biological systems. Modification of sensor compound **12** by amino acids can be achieved by following the reaction scheme shown in Scheme 4.1. After synthesizing of Fc amino acid conjugates, films could be prepared

on gold surface. The films can be fully studied and characterized as outlined in Chapters 2 and 3. It is proposed to use CV and DPV to study the sensing ability of the modified systems to CWA mimics. Titrations can be carried out on surfaces in order to quantify the sensitivity of the system upon addition of CWAs.

5. Experimental

5.1. General remarks

Trifluoroacetic acid (TFA), triethylamine (Et₃N), sodium sulphate (Na₂SO₄), sodium bicarbonate (NaHCO₃), 1-hydroxybenzotriazole hydrate (HOBT) (Advanced ChemTech), 1-(3-dimethylaminopropyl)-3-ethylcarbodiimide hydrochloride (EDC) (Advanced ChemTech), cystamine dihydrochloride (CSA) (Aldrich), methyl iodide (CH₃I) (Fisher), ethyl iodide (CH₃CH₂I), (Fisher), chloroethyl ethylsulfide (ClCH₂CH₂SEt) (Aldrich), diethyl cyanophosphonate ((CN)(EtO)₂P(O)) (Aldrich), ammonium hydroxide (NH₄OH) and potassium bromide (KBr) (IR grade, Aldrich) were used as received. All syntheses were carried out in air unless otherwise specified. CDCl₃, MeOD (Sigma-Aldrich) were stored over molecular sieves (8-12 mesh; 4 Å effective pore size; Fisher) before use. For column chromatography, a column with a width of 2.7 cm and a length of 45 cm was packed with 230-400 mesh silica gel (EM, Science). For TLC, aluminum plates coated with silica gel 60 F254 (EM, Science) were used. Boc-NH-Fc-COOMe (**1**) and BocHN-Fc-COOH (**11**) were prepared by following the literature procedure.⁹³

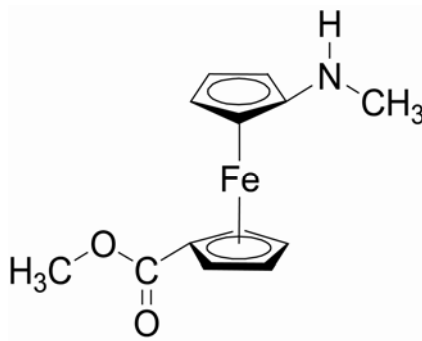
A Bruker Avance 500 MHz NMR spectrometer (¹H 500.3 MHz, ¹³C 125.8 MHz and ³¹P 202.5 MHz) equipped with a 5 mm broadband probe and dedicated ¹H, ¹³C as well as ²H for locking were employed in all experiments. Peak positions in both ¹H-NMR and ¹³C-NMR spectra are reported in ppm relative to TMS and coupling constants *J* in Hz. The ¹H-NMR spectra are referenced to residue CHCl₃ at δ 7.27 for compounds **3**, **4**, **5** and **12** and to the MeOD for compound **6**. ¹³C{¹H} spectra for compounds **3**, **4**, **5**

and **12** are referenced to the CDCl_3 signal at δ 77.23 and for compound **6** to the MeOD signal at δ 48.04. Mass spectrometry was carried out on a VG Analytical 70/20 VSE instrument. Infrared spectra were obtained on a Perkin-Elmer 1605 FT-IR (resolution: 4 cm^{-1}). UV-visible spectra were recorded on a Varian Cary 500 spectrometer.

5.2. General synthetic method for compound 3-6

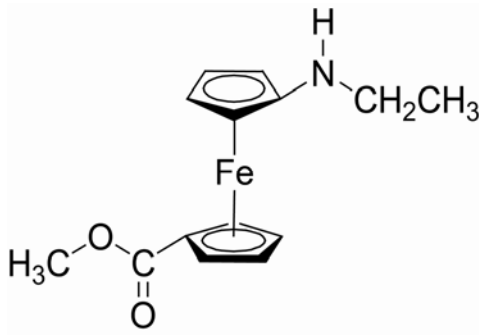
To a solution of compound **1** (100 mg, 0.29 mmol) in CH_2Cl_2 (5 ml) TFA was added under nitrogen at $0\text{ }^\circ\text{C}$ to deprotect the amino group. The mixture was stirred for 30 min and Et_3N was added to neutralize the excess TFA and to get free amine (^1H NMR (CDCl_3 , δ/ppm): 4.78 (t, Fc-2H, H-2 and H-5, $J = 4\text{ Hz}$), 4.36 (t, Fc-2H, H-2' and H-5', $J = 4\text{ Hz}$), 4.18 (d, Fc-2H, H-3 and H-4, $J = 2\text{ Hz}$), 3.98 (d, Fc-2H, H-3' and H-4', $J = 2\text{ Hz}$), 3.80 (s, COOMe-3H), 2.60 (s, NH_2)). The solvent was removed in vacuo and then dissolved in EtOH and pH was set to 9 by adding saturated NaHCO_3 solution. CH_3I , $\text{CH}_3\text{CH}_2\text{I}$, $\text{ClCH}_2\text{CH}_2\text{SEt}$ or $(\text{CN})(\text{EtO})_2\text{P}(\text{O})$ were added (0.58 mmol) and the mixture was stirred at room temperature for 3 h. Then the solution was washed with 10% citric acid solution and dried over anhydrous sodium sulfate. After evaporation of the solvent, the reaction mixture was subjected to column chromatography on SiO_2 (230-400 mesh) using hexane:ethylacetate (3:1).

5.2.1. Synthesis and Characterization of 1,*n'*-MeHN-Fc-COOMe (3)



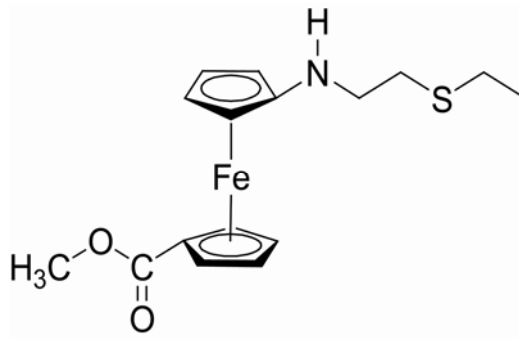
Compound **3** was synthesized by using the general procedure described above. Yield: 8 mg, 8%. EI-MS (*m/z*). Calc. for $C_{13}H_{15}NO_2Fe$ $[M+1]^+$: 273.0452. Found: 273.0453. FT-IR (KBr, cm^{-1}): 3375 (b, N-H), 1712 (s, C=O). UV-Vis (MeCN; λ in nm (ϵ in $L\ mol^{-1}\ cm^{-1}$)): 455 (106). 1H -NMR (500 MHz, $CDCl_3$, 25 °C): δ = 4.81 (t, $^3J_{H,H} = 4$ Hz, Fc-2H, H-2 and H-5), 4.38 (t, $^3J_{H,H} = 2$ Hz Fc-2H, H-2' and H-5'), 3.92 (d, $^2J_{H,H} = 2$ Hz, Fc-2H, H-3 and H-4), 3.90 (d, $^2J_{H,H} = 2$ Hz, Fc-2H, H-3' and H-4'), 3.81 (s, 1H, N-H), 3.80 (s, 3H, COOMe), 2.68 (s, 3H, amino methyl). ^{13}C -NMR (500 MHz, $CDCl_3$, 25 °C): δ = 173.0 (C=O), 71.9 (C-1, Fc), 71.5 (C-2 and C-5, Fc), 70.9 (C-1', Fc), 70.6 (C-2' and C-5', Fc), 65.1 (C-3 and C-4, Fc), 56.5 (C-3' and C-4', Fc), 51.7 (ester CH_3), 30.1 (N- CH_3).

5.2.2. Synthesis and Characterization of 1,*n'*-EtHN-Fc-COOMe (4)



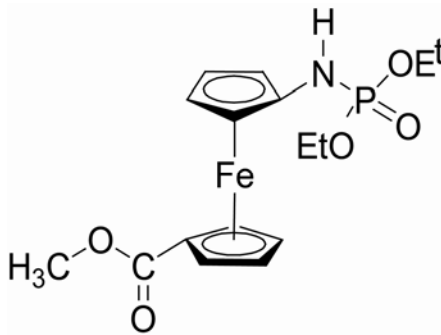
Compound **4** was synthesized by using the general procedure described above. Yield: 27 mg, 25%. EI-MS (*m/z*). Calc. for C₁₄H₁₇NO₂Fe [M+1]⁺: 287.0608. Found: 287.0610. FT-IR (KBr, cm⁻¹): 3360 (s, N-H), 1700 (s, C=O). UV-Vis (MeCN; λ in nm (ε in L mol⁻¹ cm⁻¹)): 458 (178). ¹H-NMR (500 MHz, CDCl₃, 25 °C): δ = 4.76 (s, Fc-2H, H-2 and H-5), 4.34 (s, Fc-2H, H-2' and H-5'), 3.97 (s, Fc-2H, H-3 and H-4), 3.87 (s, Fc-2H, H-3' and H-4'), 3.81 (s, 3H, COOMe), 3.79 (s, 1H, N-H), 1.35 (q, ³J_{H,H} = 14 Hz, 2H, N-CH₂), 1.23 (t, ³J_{H,H} = 14 Hz, 3H, CH₃). ¹³C-NMR (500 MHz, CDCl₃, 25 °C): δ = 171.9 (C=O), 72.8 (C-1, Fc), 72.1 (C-1', Fc), 71.3 (C-2 and C-5, Fc), 70.6 (C-2' and C-5', Fc), 65.5 (C-3 and C-4, Fc), 59.7 (C-3' and C-4', Fc), 51.8 (ester CH₃), 42.0 (N-CH₂), 30.0 (CH₃).

5.2.3. Synthesis and Characterization of 1,*n'*-EtSCH₂CH₂HN-Fc-COOMe (5)



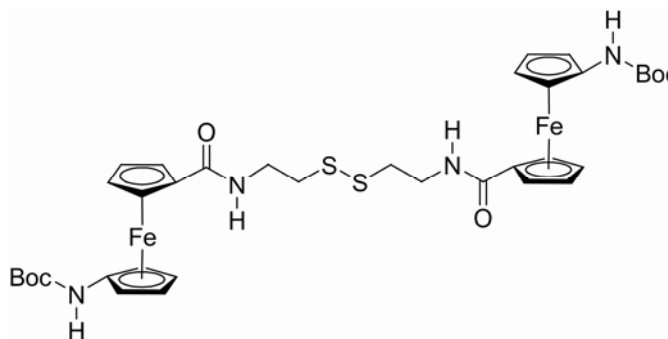
Compound **5** was synthesized by using the general procedure described above. Yield: 13 mg, 10%. EI-MS (*m/z*). Calc. for C₁₆H₂₁NO₂FeS [M+1]⁺: 347.0642. Found: 347.0637. FT-IR (KBr, cm⁻¹): 3340 (b, N-H), 1708 (s, C=O). UV-Vis (MeCN; λ in nm (ε in L mol⁻¹ cm⁻¹)): 454 (252). ¹H-NMR (500 MHz, CDCl₃, 25 °C): δ = 4.78 (t, ³J_{H,H} = 3.6 Hz, Fc-2H, H-2 and H-5), 4.38 (t, ³J_{H,H} = 4 Hz, Fc-2H, H-2' and H-5'), 3.93 (s, Fc-2H, H-3 and H-4), 3.89 (s, Fc-2H, H-3' and H-4'), 3.81 (s, 1H, N-H), 3.80 (s, 3H, COOMe), 3.12 (s, 2H, N-CH₂), 2.80 (t, ³J_{H,H} = 13 Hz, 2H, S-CH₂), 2.64 (q, ³J_{H,H} = 22 Hz, 2H, S-CH₂), 1.33 (t, ³J_{H,H} = 15 Hz, 3H, S-CH₃). ¹³C-NMR (500 MHz, CDCl₃, 25 °C): δ = 172.2 (C=O), 72.9 (C-1, Fc), 72.5 (C-1', Fc), 71.4 (C-2 and C-5, Fc), 70.2 (C-2' and C-5', Fc), 64.9 (C-3 and C-4, Fc), 56.7 (C-3' and C-4', Fc), 51.4 (ester CH₃), 45.5 (N-CH₂), 31.7 (S-CH₂), 25.8 (S-CH₂), 14.9 (CH₃).

5.2.4. Synthesis and Characterization of 1,*n'*-(EtO)₂P(O)NH-Fc-COOMe (6)



Compound **6** was synthesized by using the general procedure described above at a temperature of $-20\text{ }^{\circ}\text{C}$. Yield: 68 mg, 8%. EI-MS (m/z). Calc. for $\text{C}_{16}\text{H}_{22}\text{NO}_5\text{PFe}$ $[\text{M}+1]^+$: 395.0584. Found: 395.0574. FT-IR (KBr, cm^{-1}): 3245 (b, N-H), 1720 (s, C=O), 1500 (s, P-O). UV-Vis (MeCN; λ in nm (ϵ in $\text{L mol}^{-1} \text{cm}^{-1}$)): 451 (144). ^1H -NMR (500 MHz, MeOD, $25\text{ }^{\circ}\text{C}$): $\delta = 4.78$ (s, Fc-2H, H-2 and H-5), 4.6 (s, Fc-2H, H-2' and H-5'), 4.4 (s, Fc-2H, H-3 and H-4), 4.0 (s, Fc-2H, H-3' and H-4'), 4.1 (q, $^3J_{\text{H,H}} = 7\text{ Hz}$, 2H, O-CH₂), 3.99 (s, 1H, N-H), 3.80 (s, 3H, COOMe), 1.25 (t, $^3J_{\text{H,H}} = 7\text{ Hz}$, 3H, CH₃). ^{13}C -NMR (500 MHz, MeOD, $25\text{ }^{\circ}\text{C}$): $\delta = 172.0$ (C=O), 73.2 (C-1, Fc), 71.0 (C-1', Fc), 69.8 (C-2 and C-5, Fc), 66.8 (C-2' and C-5', Fc), 64.2 (C-3 and C-4, Fc), 60.5 (C-3' and C-4', Fc), 51.1 (ester CH₃), 34.7 (CH₂), 25.2 (CH₃). $^{31}\text{P}\{^1\text{H}\}$ -NMR (500 MHz, MeOD, $25\text{ }^{\circ}\text{C}$): $\delta = 48.7$.

5.2.5. Synthesis and Characterization of [BocNH-Fc-CO-CSA]₂ (12)



To a stirring mixture of BocHN-Fc-COOH (**11**) (50 mg, 0.14 mmol) and HOBT (33 mg, 0.22 mmol) in CH₂Cl₂ (10 mL), solid EDC was added (42 mg, 0.22 mmol) at 0°C and stirring was continued for 3 hrs. A slurry of cystamine dihydrochloride (6 mg; 0.05 mmol) in CH₂Cl₂ (10 mL) followed by Et₃N (0.5 mL) was added to the reaction mixture and stirring was continued for 10 hrs at room temperature. The yellow reaction mixture was then subjected to an aqueous work up by washing with sat. NaHCO₃ and 10% citric acid and again with sat. NaHCO₃. After drying of the organic phase over anhydrous Na₂SO₄, the solvent was evaporated to dryness and the residue was chromatographed on silica (n-hexane: EtOAc: MeOH 5:4:1; R_f = 0.30), giving the desired orange product in 83% yield (35 mg). UV-vis (CH₃CN, λ_{max} in nm, ε in Lmol⁻¹ cm⁻¹): 442 (366). IR (KBr, cm⁻¹): 3441 (NH), 3334 (NH), 2976 (Fc), 2927 (CH₃), 1710 (C=O), 1639 (Amide I), 1533 (Amide II), 1390 (Cp), 1247 (C-O). ¹H-NMR (500 MHz, CDCl₃, 293 K): δ 7.27 (s, 1H, N-H, CSA amide), 6.39 (s, 1H, N-H, Boc-NH), 4.72 (s, 2H, Fc-H), 4.42 (s, 2H, Fc-H), 4.36 (s, 2H, Fc-H), 4.05 (s, 2H, Fc-H), 3.76 (t, 2H, N-CH₂, J = 5 Hz), 3.02 (t, 2H, S-CH₂, J = 5 Hz), 1.51 (s, 9H, Boc). ¹³C{¹H}-NMR (500

MHz, CDCl₃, 293 K): δ 171.3 (C=O CSA amide), 154.3 (Boc-C=O), 96.8 (Boc-tert-C), 80.8 (ipso-C, Fc-C(O)), 78.2 (ipso-C, Fc-NH), 71.4, 69.9, 66.2, 63.5 (Fc-C), 39.4 (CH₂-N), 38.6 (CH₂-S), 28.8 (CH₃). ESI-MS: exact mass m/z calcd. for C₃₆H₄₆O₆N₄Fe₂S₂ 806.1557, found 806.1767. Anal. Calc. for C₃₆H₄₆O₆N₄Fe₂S₂: C, 53.60; H, 5.70; N, 6.94. Found: C, 53.03; H, 5.69; N, 6.87%.

5.3. Electrochemical measurements

The electrochemical experiments were carried out at room temperature using CHI 660b Instruments. A glassy carbon electrode (BAS, diameter 2 mm) was used as working electrode and Pt wire as counter electrode while Ag/AgCl (BAS) was used as a reference electrode. The glassy carbon electrode was polished with 3 μ m alumina powder followed by 1 μ m, then 0.5 μ m alumina prior to use to remove any surface contamination. 1 mM solution of the compounds in CH₃CN was prepared and 0.2 M tetrabutylammonium perchlorate (TBAP) was used as supporting electrolyte. The cyclic voltammetry measurements were carried out at a scan rate of 100 mV/s (8 scan cycle).

5.4. Quantum mechanical calculations

Standard molecular orientations were used in building the molecules of compounds 2–6 using the program SPARTAN-04. The geometries were partially optimized using the Spartan minimizer. Complete optimization of the molecules was performed using GAUSSIAN-03⁹⁴ in C₁ using the DFT/B3LYP method with 6-31G** basis set. Electron density on ferrocene was calculated from natural bond orbital analysis for all the optimized structures at the same theoretical level. The molecular orbital diagrams

were constructed using ArgusLab.⁹⁵ The molecular orbital data generated by GaussView was input into ArgusLab and the final images created using the ray tracing program POV-RAY 3.5.

5.5. Film Preparation and Surface Electrochemistry

Gold microelectrodes having a diameter of 25 μm were prepared and surface roughness was determined by Cu UPD^{96,97} and was in the range of 1.2 – 1.4 for all electrodes. Thin films were prepared by soaking the microelectrodes in a 1mM ethanolic solution of compound **12** for 5 days. The modified surfaces were washed with copious amounts of ethanol, Millipore water and then sonicated in ethanol solution for 2 sec and again rinsed with Millipore water. The film was then backfilled by incubating the electrodes for 5 min in 1 mM ethanolic solution of butanethiol. Deprotection of Boc-amine was carried out by exposing the film to 40% TFA in DCM for 1 min and subsequent washing with absolute ethanol, then to Millipore water and finally exposing to 10% NH_4OH in H_2O for 15 sec. Again the electrodes were washed with Millipore water and placed back in 2M NaClO_4 electrolyte solution for electrochemical measurements.⁹⁸

All electrochemical measurements were carried out using a CHI Instrument 660b electrochemical workstation. 2.0 M NaClO_4 was used as the supporting electrolyte. An Ag/AgCl (3M KCl)-electrode served as the reference electrode and a Pt wire as the counter electrode. For cyclic voltammetry (CV) experiments, the scan rate was 100 V/s. After each modification the surface was given 2 min rest time before any electrochemical signal was recorded. Differential Pulse Voltammetry (DPV)

measurements were carried out by setting the amplitude at 0.05 V with a pulse width of 0.05 s and pulse period of 0.2 s.

5.6. Ellipsometry Study

Film thickness was measured using an LSE Stokes ellipsometer (Gaertner Scientific Corporation, Skokie, IL) with a fixed angle of 70° and a fixed wavelength of 632.8 nm and a HeNe Laser as a light source. The data were collected and analyzed using LGEMP (Gaertner Ellipsometer Measurement Software) on a PC. Au on Si(100) (Platypus Technologies, Inc.) wafers were used as a substrate with refractive index $N_s = 0.133$, absorption index $K_f = 3.462$ and film refractive index was set to 1.44.

5.7. Quartz Crystal Microbalance (QCM) Measurements

QCM experiments were conducted on a CHI 440 (CH Instruments Inc.) using quartz crystals (8 MHz, AT-cut, diameter 9 mm) covered with Au (1000 Å) on a Ti adhesion layer (100 Å), commercially available from CH Instruments). The QCM experiment relies on the calculation of mass change (Δm) at the quartz crystal using measured frequency change (Δf) according to the Sauerbrey equation (Eq. 1):

$$\Delta f = \frac{-2f_0^2}{A\sqrt{\mu\rho}} \Delta m \quad (1)$$

where f_0 is the resonant frequency of the fundamental mode of the crystal, A the area of the gold disk coated onto the crystal (0.205 cm² for given crystal), ρ the density of the

crystal and μ the shear modulus of quartz. The density of the crystal is 2.648 g/cm^3 and the shear modulus μ is $2.947 \times 10^{11} \text{ g/cm s}^2$. For 8 MHz crystal, the mass change is 0.14 ng for 0.1 Hz frequency change.

The preparation of the films on the crystals was analogous to that described for the other surfaces, soaking the crystals for five days in a 1 mM ethanolic solution of compound **12**, followed by washing with ethanol, Millipore water, and drying under a stream of nitrogen. All QCM experiments were carried out under an argon atmosphere to protect the films from atmospheric moisture. The mass of the compound **12** on quartz crystal was arbitrarily taken as zero and its frequency is taken as baseline frequency for the experiments.

5.8. X-ray Photoelectron Spectroscopy (XPS)

XPS was carried out on Kratos (AEI) DS300 instrument, using the Mg K lines for excitation at the University of Alberta. The specimen was mounted on a double-stick scotch tape. The position of core levels was calibrated relative to the gold $4f_{7/2}$ line (assumed to be at 83.8 eV). Samples were prepared by treating the gold substrate (commercially available from CH Instruments Inc.) with piranha solution (70% conc. $\text{H}_2\text{SO}_4 + 30\% \text{ H}_2\text{O}_2$. **Caution: Piranha solution is highly oxidizing and any direct contact should be avoided**) to remove any organic contaminants. It was then washed with copious amount of water and ethanol, dried over argon and then soaked in a 1mM ethanolic solution of compound **12** for five days. Deprotection of compound **12** was carried out as described before. For **12-d+MA** and **12-d+NA**, substrates were exposed

to MA and NA for another 2 min. All substrates were stored in an argon atmosphere before doing the XPS measurements.

5.9. X-ray crystallography

Suitable crystals of compound **12** (orange plate; 0.20 × 0.13 × 0.10 mm) were obtained from a chloroform solution by slow evaporation of the solvent. All measurements were made on a Nonius Kappa CCD 4-Circle Kappa FR540C diffractometer using monochromated Mo K α radiation ($\lambda=0.71073$ Å) at -100 °C. An initial orientation matrix and cell was determined from 10 frames using ϕ -scans. Data reduction was performed with the HKL DENZO and SCALEPACK software.⁹⁹ The structure was solved using direct methods (SHELXS-97)¹⁰⁰ and refined by full-matrix least-squares method on F^2 (SHELXL97-2).¹⁰¹ The non-hydrogen atoms were refined anisotropically. Hydrogen atoms were included at geometrically idealized positions (C-H bond distances 0.95/0.99 Å; N-H bond distance 0.88 Å) and were not refined. The isotropic thermal parameters of the hydrogen atoms were fixed at 1.2 times that of the preceding carbon or nitrogen atom. The structure contains two severely disordered CHCl₃ solvent molecules per asymmetric unit. It was possible to model the disorder of one solvent molecule with higher than usual principal mean square atomic displacement parameters. Attempts to refine peaks of residual electron density as water were unsuccessful. The data were corrected for disordered electron density through use of the SQUEEZE¹⁰² procedure as implemented in PLATON.¹⁰³ A total solvent-accessible void volume of 389.3 Å³ (16% of the unit cell volume) with a total electron count of 85 was

found in the unit cell. Derived values (formula weight, density, absorption coefficient) do not contain the contribution of the disordered solvent molecule.

Table 5.1. Crystal data and refinement of compound **12** × CHCl₃

Empirical formula	C ₃₇ H ₄₇ Cl ₃ Fe ₂ N ₄ O ₆ S ₂
Formula weight	925.96
Temperature	173(2) K
Wavelength	0.71073 Å
Crystal system	Triclinic
Space group	P-1 [No. 2]
Unit cell dimensions	
a, Å	11.8954(3)
b, Å	13.3664(4)
c, Å	16.6714(5)
α, deg	85.6016(16)
β, deg	79.355(16)
γ, deg	69.3280(16)
V, Å ³	2437.19(12)
D _{calc} , g/m ³	1.262
Crystal size, mm	0.20 × 0.13 × 0.10
θ range for data collection	2.00 to 26.40°
Goodness-of-fit (F ₂)	1.046
R1 [I > 2σ (I)] ^a	0.0512
wR2 (all data) ^b	0.1548
aR1 = [Σ F _o - F _c]/[Σ F _o] for [I > 2σ (I)]	
bWR2 = {[Σw(F _o ² - F _c ²) ²]/ [Σw(F _o ²) ²]} ^{1/2} all data	

The hydrogen atom at the carbon atom of the CHCl₃ solvent molecule was located in Fourier difference map. Its coordinates were allowed to refine, whereas its isotropic thermal parameter was fixed at 1.2 times that of the preceding carbon atom. The final cycle of full-matrix least squares refinement using F^2 (SHELXL 97-2) was based on

6238 reflections, 348 variable parameters and converged with $R_1 = 0.0375$ for $I > 2\sigma(I)$.
Crystallographic details for **12** (CCDC reference number 602112) are provided in Table 5.1.

References

- (1) Somani, S. M. *Chemical Warfare Agents*; Academic Press: London, 1992.
- (2) Black, R. M.; Clarke, R. J.; Read, R. W.; Reid, M. T. J. *J. Chromatogr. A* **1994**, *662*, 301-321.
- (3) Nozaki, H.; Aikawa, N. *Lancet* **1995**, *345*, 1446-1447.
- (4) Bismuth, C.; Borron, S. W.; Baud, F. J.; Barriot, P. *Toxicol. Lett.* **2004**, *149*, 11-18.
- (5) Wingfield, T. *Military Law Review* **1999**, *162*, 180-219.
- (6) Sugendran, P.; Kumar, R.; Vijayaraghavan *Defense Sci. J.* **1998**, *48*, 155-162.
- (7) Sadik, O. A.; Land, J. W. H.; Wang, J. *Electroanalysis* **2003**, *15*, 1149-1159.
- (8) In *The Chemical Weapons Conventions: Implementation Challenges and Solutions*; Tucker, J. B., Ed.; Monterey Institute of International Studies: Washington, D. C., USA, 2001.
- (9) Bartlett, P. D.; Swain, C. G. *J. Am. Chem. Soc.* **1949**, *71*, 1406-1415.
- (10) Munro, N. B.; Talmage, S. S.; Griffin, G. D.; Waters, L. C.; Watson, A. P.; King, J. F.; Hauschild, V. *Environ. Health Perspect.* **1999**, *107*, 933-974.
- (11) Epstein, J.; Callahan, J. J.; Bauer, V. E. *Phosphorus* **1974**, *4*, 157-163.
- (12) Kingery, A. F.; Allen, H. E. *Toxicol. Environ. Chem.* **1995**, *47*, 155-184.
- (13) Nassar, A.-E. F.; Lucas, S. V.; Jones, W. R.; Hoffland, L. D. *Anal. Chem.* **1998**, *70*, 1085-1091.
- (14) Wormser, U. *Trends Pharmacol. Sci.* **1991**, *12*, 164-167.
- (15) Fitch, J. P.; Raber, E.; Imbro, D. R. *Science* **2003**, *302*, 1350-1355.
- (16) Noort, D.; Hulst, A. G.; Jansen, R. *Arch. Toxicol.* **2002**, *76*, 83-88.

- (17) Stewart, C. E.; Sullivan Jr., J. B. In *Hazardous Materials Toxicology : Clinical Principles Of Environmental Health*; Sullivan Jr., J. B., Krieger, G. R., Eds.; Williams and Wilkins: Baltimore, 1992, p 986-1014.
- (18) Xie, Y.; Popov, B. N.; White, R. E. *J. Electroanal. Chem.* **1999**, *466*, 169-176.
- (19) Mulchandani, A.; Mulchandani, P.; Chen, W.; Wang, J.; Chen, L. *Anal. Chem.* **1999**, *71*, 2246-2249.
- (20) Guodong, L.; Lin, Y. *Anal. Chem.* **2006**, *78*, 835-843.
- (21) Nassar, A.-E. F.; Lucas, S. V.; Myler, C. A.; Jones, W. R.; Campisano, M.; Hoffland, L. D. *Anal. Chem.* **1998**, *70*, 3598-3604.
- (22) Rosso, T. E.; Bossle, P. C. *J. Chromatogr. A* **1998**, *824*, 125-134.
- (23) Kavallieratos, K.; Hwang, S.; Crabtree, R. H. *Inorg. Chem.* **1999**, *38*, 5184-5186.
- (24) Wang, J.; Zima, J.; Lawrence, N. S.; Chatrathi, M. P.; Mulchandani, A.; Collins, G. E. *Anal. Chem.* **2004**, *76*, 4721-4726.
- (25) Xie, Y.; Popov, B. N. *Anal. Chim. Acta.* **2001**, *448*, 221-230.
- (26) Xie, Y.; Popov, B. N. *Anal. Chem.* **2000**, *72*, 2075-2079.
- (27) Hsueh, C.-C.; Liu, Y.; Freund, M. S. *Anal. Chem.* **1999**, *71*, 4075-4080.
- (28) Mulchandani, P.; Chen, W.; Mulchandani, A. *Environ. Sci. Technol.* **2001**, *35*, 2562-2565.
- (29) Arribas, A. S.; Vázquez, T.; Wang, J.; Mulchandani, A.; Chen, W. *Electrochem. Comm.* **2005**, *7*, 1371-1374.
- (30) Joshi, K. A.; Prouza, M.; Kum, M.; Wang, J.; Tang, J.; Haddon, R.; Chen, W.; Mulchandani, A. *Anal. Chem.* **2006**, *78*, 331-336.
- (31) Shulga, O. V.; Palmer, C. *Anal. Bioanal. Chem.* **2006**, *385*, 1116-1123.

- (32) Joshi, K. A.; Tang, J.; Haddon, R.; Wang, J.; Chen, W.; Mulchandani, A. *Electroanalysis* **2005**, *17*, 54-58.
- (33) Schöning, M. J.; Arzdorf, M.; Mulchandani, P.; Chen, W.; Mulchandani, A. *Sensors and Actuators B* **2003**, *91*, 92-97.
- (34) Cecchet, F.; Pilling, M.; Hevesi, L.; Schergna, S.; Wong, J. K. Y.; Clarkson, G. J.; Leigh, D. A.; Rudolf, P. *J. Phys. Chem.* **2003**, *107*, 10863-10872.
- (35) Hopkins, A. R.; Lewis, N. S. *Anal. Chem.* **2001**, *73*, 884-892.
- (36) Zhou, Y.; Yu, B.; Shiu, E.; Levon, K. *Anal. Chem.* **2004**, *76*, 2689-2693.
- (37) Guodong, L.; Lin, Y. *Anal. Chem.* **2005**, *77*, 5894-5901.
- (38) Carr, J. D.; Lambert, L.; Hibbs, D. E.; Hursthouse, M. B.; Abdul Malik, K. M.; Tucker, J. H. R. *Chem. Comm.* **1997**, *17*, 1649-1650.
- (39) Carr, J. D.; Coles, S. J.; Hassan, W. W.; Hursthouse, M. B.; Abdul Malik, K. M.; Tucker, J. H. R. *J. Chem. Soc. Dalton Trans.* **1999**, *1*, 57-62.
- (40) Appoh, F. E.; Sutherland, T. C.; Kraatz, H. B. *J. Organomet. Chem.* **2005**, *690*, 1209-1217.
- (41) Beer, P. D.; Davis, J. J.; Drillsma-Milgrom, D. A.; Szemes, F. *Chem. Commun.* **2002**, *16*, 1716-1717.
- (42) Brindley, G. D.; Fox, O. D.; Beer, P. D. *J. Chem. Soc. Dalton Trans.* **2000**, *23*, 4354-4359.
- (43) Delavaux-Nicot, B.; Fery-Forgues, S. *Eur. J. Inorg. Chem.* **1999**, *1999*, 1821-1825.
- (44) Kuo, L.-J.; Liao, J.-H.; Chen, C.-T.; Huang, C.-H.; Chen, C.-S.; Fang, J.-M. *Org. Lett.* **2003**, *5*, 1821-1824.

- (45) Chen, Z.; Pilgrim, A. J.; Beer, P. D. *J. Electroanal. Chem.* **1998**, *444*, 209-217.
- (46) Beer, P. D.; Chen, Z.; Pilgrim, A. J. *J. Chem. Soc. Faraday Trans.* **1995**, *91*, 4331-4333.
- (47) Hall, C. D.; Chu, S. Y. F. *J. Organomet. Chem.* **1995**, *498*, 221-228.
- (48) Duffy, N. W.; Harper, J.; Ramani, P.; Ranatunge-Bandarage, R.; Robinson, B. H.; Simpson, J. *J. Organomet. Chem.* **2004**, *564*, 125-131.
- (49) Gao, Y.; Twamley, B.; Shreeve, J. M. *Inorg. Chem.* **2004**, *43*, 3406-3412.
- (50) van Staveren, D. R.; Weyhermüller, T.; Metzler-Nolte, N. *Dalton Trans.* **2003**, 210-220.
- (51) Liang, G.-B.; Dado, G. P.; Gellman, S. H. *J. Am. Chem. Soc.* **1991**, *113*, 3994-3995.
- (52) Gellman, S. H.; Dado, G. P.; Liang, G.-B.; Adams, B. R. *J. Am. Chem. Soc.* **1991**, *113*, 1164-1173.
- (53) Bradley, S.; McGowan, P. C.; Oughton, K. A.; Camm, K. D.; Liu, X.; Mumtaz, R.; Podesta, T. J.; Thornton-Pett, M. *Inorg. Chem.* **2002**, *41*, 715-726.
- (54) Mahmoud, K.; Long, Y. T.; Schatte, G.; Kraatz, H. B. *J. Organomet. Chem.* **2004**, *689*, 2250-2255.
- (55) Atkinson, R. C. J.; Gibson, V. C.; Long, N. J.; White, A. J. P.; Williams, D. J. *Dalton Trans.* **2004**, 1823-1826.
- (56) Longlet, J. J.; Bodige, S. G.; Watson, W. H.; Neilson, R. H. *Inorg. Chem.* **2002**, *41*, 6507-6513.
- (57) Robinson, B. H.; Simpson, J.; Wilson, D. J. *Acta Cryst.* **1996**, *C52*, 2196-2198.

- (58) Hocek, M.; Stepnicka, P.; Ludvik, J.; Cisarova, I.; Votruba, I.; Reha, D.; Hobza, P. *Chem. Eur. J.* **2004**, *10*, 2058-2066.
- (59) König, W.; Geiger, R. *Chem. Ber.* **1970**, *103*, 788-798.
- (60) Barišić, L.; Dropučić, M.; Rapić, V.; Pritzkow, H.; Kirin, S. I.; Metzler-Nolte, N. *Chem. Comm.* **2004**, 2004-2005.
- (61) Bediako-Amoa, I.; Sutherland, T. C.; Li, C.-Z.; Silerova, R.; Kraatz, H.-B. *J. Phys. Chem. B* **2004**, *108*, 704-714.
- (62) Brauner, J. W.; Dugan, C.; Mendelsohn, R. *J. Am. Chem. Soc.* **2000**, *122*, 677-683.
- (63) Gu, Z.; Zambrano, R.; Mcdermott, A. *J. Am. Chem. Soc.* **1994**, *116*, 6368-6372.
- (64) Tonan, K.; Ikawa, S.-i. *J. Am. Chem. Soc.* **1996**, *118*, 6960-6965.
- (65) Toniolo, C.; Bonora, G. M.; Marchiori, F.; Borin, G. *J. Am. Chem. Soc.* **1984**, *106*, 1455-1457.
- (66) Holovics, T. C.; Deplazes, S. F.; Toriyama, M.; Powell, D. R.; Lushington, G. H.; Baryin, M. V. *Organometallics* **2004**, *23*, 2927-2938.
- (67) Heinze, K.; Schlenker, M. *Eur. J. Inorg. Chem.* **2004**, 2974-2988.
- (68) Okamura, T.; Sakauye, K.; Ueyama, N.; Nakamura, A. *Inorg. Chem.* **1998**, *37*, 6731-6736.
- (69) Clark, R. A.; Bowden, E. F. *Langmuir* **1997**, *13*, 559-565.
- (70) Sabapathy, R. C.; Bhattacharyya, S.; Leavy, M. C.; Cleland Jr., W. C.; Hussey, C. L. *Langmuir* **1998**, *14*, 124-136.
- (71) Fawcett, W. R. *J. Electroanal. Chem.* **1994**, *378*, 117-124.
- (72) Smith, C. P.; White, H. S. *Anal. Chem.* **1992**, *64*, 2398-2405.

- (73) Rowe, G. K.; Creager, S. E. *Langmuir* **1991**, *7*, 2307-2312.
- (74) Clark, R. A.; Bowden, E. F. *langmuir* **1997**, *13*, 559-565.
- (75) Bain, C. D.; Biebuyck, H. A.; Whitesides, G. M. *Langmuir* **1989**, *5*, 723-727.
- (76) Okahata, Y.; Matsuura, K.; Ito, K.; Ebara, Y. *Langmuir* **1996**, *12*, 1023-1026.
- (77) Cheng, T.-J.; Lin, T.-M.; Chang, H.-C. *Anal. Chim. Acta* **2002**, *462*, 261-273.
- (78) Menz, B.; Knerr, R.; Gopferich, A.; Steinem, C. *Biomaterials* **2005**, *26*, 4237-4243.
- (79) Marx, K. A.; Zhou, T.; Long, D. *Biomacromolecules* **2005**, *6*, 1698-1706.
- (80) Castner, D. G.; Hinds, K.; Grainger, D. W. *Langmuir* **1996**, *12*, 5083-5086.
- (81) Evans, S. D.; Goppert-Beraducci, K. E.; Urankar, E.; Gerenser, L. J.; Ulman, A.; Snyder, R. G. *Langmuir* **1991**, *7*, 2700-2709.
- (82) Hutt, D. A.; Leggett, G. J. *J. Phys. Chem. B* **1996**, *100*, 6657-6662.
- (83) Laibinis, P. E.; Whitesides, G. M.; Allara, D. L.; TAO, Y.-T.; Parikh, A. N.; Nuzzo, R. G. *J. Am. Chem. Soc.* **1991**, *113*, 7152-7167.
- (84) Sun, F.; Castner, D. G.; Mao, G.; Mckeown, P.; Grainger, D. W. *J. Am. Chem. Soc.* **1996**, *118*, 1856-1866.
- (85) Sun, F.; Grainger, D. W.; Castner, D. G.; Leach-Scampavia, D. K. *Macromolecules* **1994**, *27*, 3053-3062.
- (86) Walczak, M. M.; Alves, C. A.; Lamp, B. D.; Porter, M. D. *J. Electroanal. Chem.* **1995**, *396*, 103-114.
- (87) Zubrägel, C.; Deuper, C.; Scheider, F.; Neumann, M.; Grunze, M.; Schertel, A.; Woll, C. *Chem. Phys. Lett.* **1995**, *238*, 308-312.

- (88) Bagno, A.; Claeson, S.; Maggini, M.; Martini, M. L.; Prato, M.; Scorrano, G. *Chem. Eur. J.* **2002**, *8*, 1015-1023.
- (89) Adenier, A.; Chehimi, M. M.; Gallrdo, I.; Pinson, J.; Vila, N. *Langmuir* **2004**, *20*, 8243-8253.
- (90) Black, R. M.; Harrison, J. M.; Read, R. W. *Xenobiotica* **1997**, *27*, 11-32.
- (91) Sandelowsky, I.; Simon, G. A.; Bel, P.; Barak, R.; Vincze, A. *Arch. Toxicol.* **1992**, *66*, 296-297.
- (92) van der Schans, G. P.; Noort, D.; Mars-Groenendijk, R. H.; Fidder, A.; Chau, L. F.; De Jong, L. P. A.; Benschop, H. P. *Chem. Res. Toxicol.* **2002**, *15*, 21-25.
- (93) Barišić, L.; Rapić, V.; Kovač, V. *Croatia Chemica Acta* **2002**, *75*, 199-210.
- (94) Gaussian 03, R. C.; Frisch, M. J.; Trucks, G. W.; Schlegel, H. B.; Scuseria, G. E.; Robb, M. A.; Cheeseman, J. R.; Montgomery, J., J. A.; Vreven, T.; Kudin, K. N.; Burant, J. C.; Millam, J. M.; Iyengar, S. S.; Tomasi, J.; Barone, V.; Mennucci, B.; Cossi, M.; Scalmani, G.; Rega, N.; Petersson, G. A.; Nakatsuji, H.; Hada, M.; Ehara, M.; Toyota, K.; Fukuda, R.; Hasegawa, J.; Ishida, M.; Nakajima, T.; Honda, Y.; Kitao, O.; Nakai, H.; Klene, M.; Li, X.; Knox, J. E.; Hratchian, H. P.; Cross, J. B.; Bakken, V.; Adamo, C.; Jaramillo, J.; Gomperts, R.; Stratmann, R. E.; Yazyev, O.; Austin, A. J.; Cammi, R.; Pomelli, C.; Ochterski, J. W.; Ayala, P. Y.; Morokuma, K.; Voth, G. A.; Salvador, P.; Dannenberg, J. J.; Zakrzewski, V. G.; Dapprich, S.; Daniels, A. D.; Strain, M. C.; Farkas, O.; Malick, D. K.; Rabuck, A. D.; Raghavachari, K.; Foresman, J. B.; Ortiz, J. V.; Cui, Q.; Baboul, A. G.; Clifford, S.; Cioslowski, J.; Stefanov, B. B.; Liu, G.; Liashenko, A.; Piskorz, P.; Komaromi, I.; Martin, R. L.; Fox, D. J.; Keith, T.; Al-Laham, M. A.; Peng, C. Y.; Nanayakkara, A.; Challacombe, M.; Gill, P. M. W.;

Johnson, B.; Chen, W.; Wong, M. W.; Gonzalez, C.; Pople, J. A.; Gaussian, I., Wallingford CT. **2004**.

(95) Thompson, M. A.; 4.0.1 ed.; Planaria Software LLC: Seattle, WA, 2005.

(96) Schneeweiss, M. A.; Kolb, D. M. *Phys. Stat. Sol.* **1999**, *173*, 51-71.

(97) Uchida, H.; Hiei, M.; Watanabe, M. *J. Electroanal. Chem.* **1998**, *452* 97–106.

(98) Carr, J. D.; Lambert, L.; Hibbs, D. E.; Hursthouse, M. B.; Abdul Malik, K. M.; Tucker, J. H. R. *Chem. Commun.* **1997**, *17*, 1649-1650.

(99) Otwinowski, Z.; Minor, W. In *Volume 276: Macromolecular Crystallography, Part A*; HKL DENZO and SCALEPACK vl. 96 ed.; Carter, C. W., Sweet Jr., R. M., Eds.; Academic Press: San Diego, CA, 1997; Vol. 276, p 307-326.

(100) Sheldrick, G. M.; SHELXS-97, Program for the Solution of Crystal Structures University of Göttingen: Göttingen, Germany, 1997.

(101) Sheldrick, G. M.; SHELXS97-2, Program for the Solution of Crystal Structures University of Göttingen: Göttingen, Germany, 1997.

(102) Sluis, P. V. D.; Spek, A. L. *Acta Crystallogr.* **1990**, *46A*, 194-201.

(103) Spek, A. L.; PLATON: A Multipurpose Crystallographic Tool ed.; Utrecht University: Utrecht, The Netherlands, 1998.

Appendix

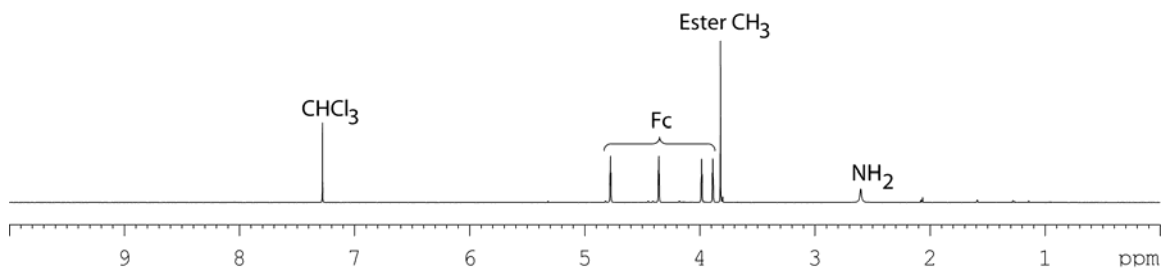


Figure A1. ¹H-NMR spectrum of 1, *n*'-NH₂-Fc-COOMe (**2**) in CDCl₃ at room temperature with full peak assignment.

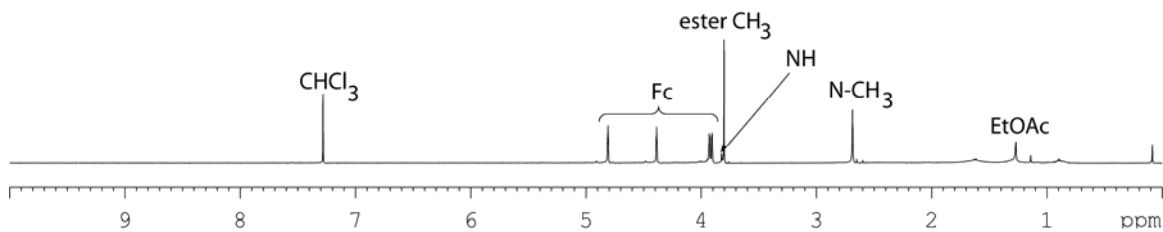


Figure A2. ¹H-NMR spectrum of 1, *n*'-MeHN-Fc-COOMe (**3**) in CDCl₃ at room temperature with full peak assignment.

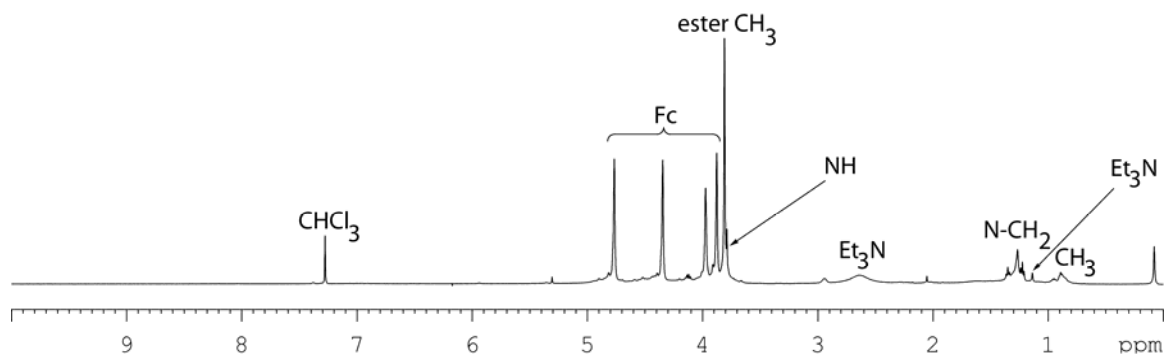


Figure A3. $^1\text{H-NMR}$ spectrum of $1,n'$ -EtHN-Fc-COOMe (**4**) in CDCl_3 at room temperature with full peak assignment.

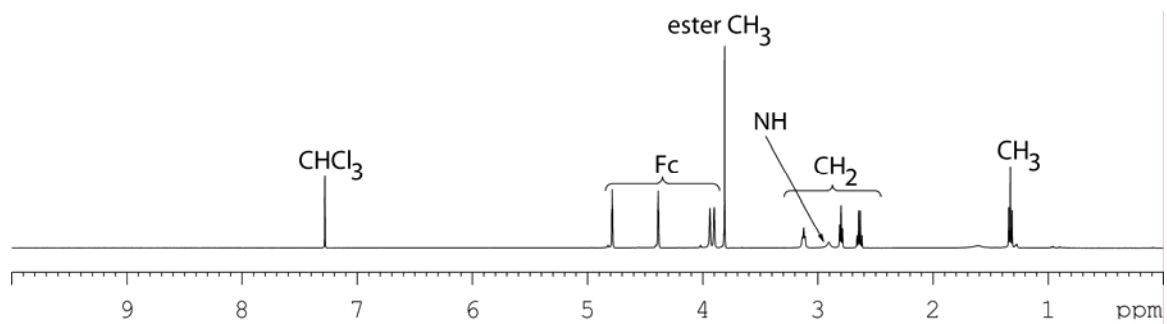


Figure A4. $^1\text{H-NMR}$ spectrum of $1,n'$ -EtSCH₂CH₂HN-Fc-COOMe (**5**) in CDCl_3 at room temperature with full peak assignment.

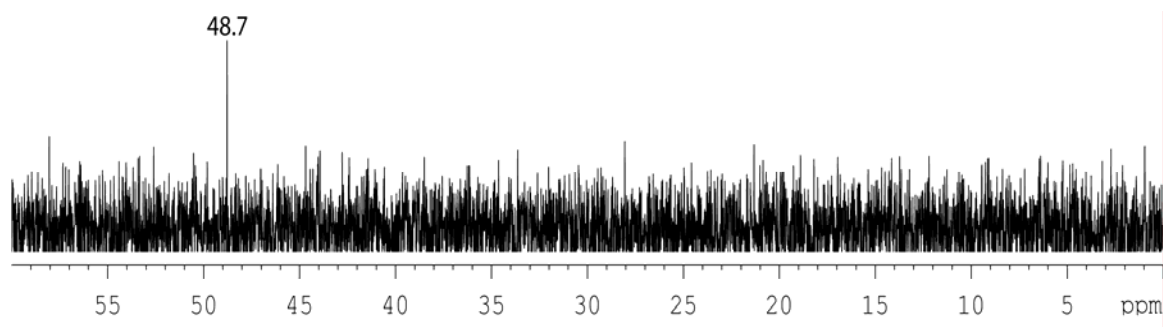


Figure A5. ^{31}P NMR spectrum of 1, n' -(EtO) $_2$ P(O)NH-Fc-COOMe (**6**) in MeOD at room temperature.

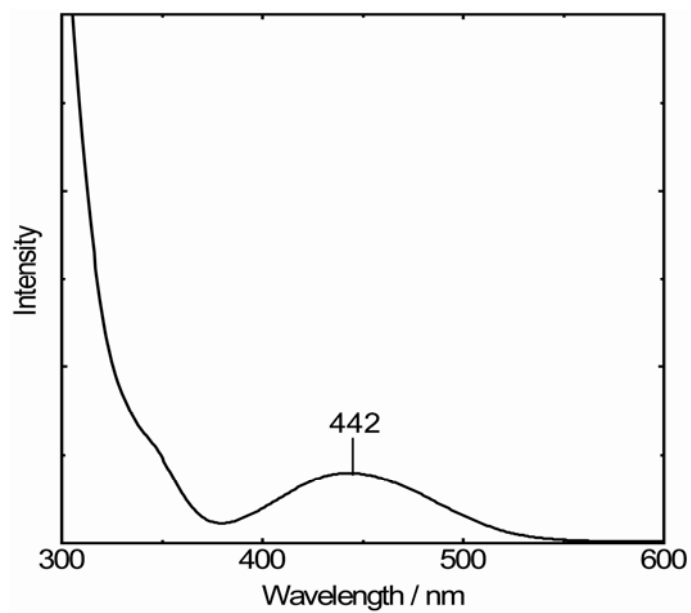


Figure A6. UV-visible spectrum of [BocNH-Fc-CO-CSA] $_2$ (**12**) in CH $_3$ CN at room temperature.

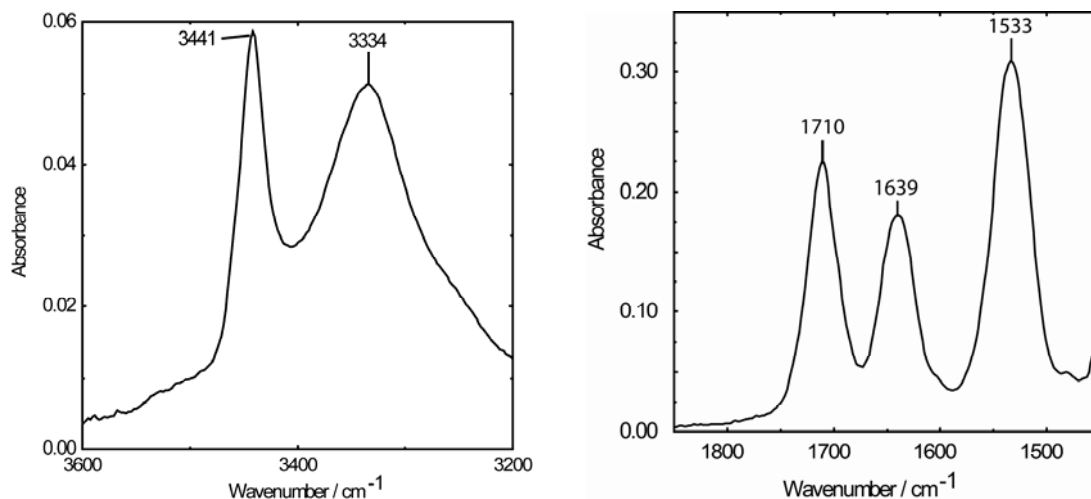


Figure A7. Partial IR spectrum of $[\text{BocNH-Fc-CO-CSA}]_2$ (**12**) in KBr at room temperature with band assignment.

Reflectance-Absorbance Infrared Spectroscopy (RAIRS) study of compound **12** on Au surface

All infrared spectra were obtained using a Thermo Nicolet Nexus 870 FT-IR with a liquid nitrogen-cooled, wide-band mercury cadmium telluride detector. Each spectrum was obtained by averaging 50000 interferograms at 4 cm^{-1} resolution with *p*-polarized light incident on the gold substrate at 80° . Each substrate was purged with CO_2 free dry air for at least 2 hours. Fresh gold substrate was used to get the reference spectrum. Peaks at 2925 and 2852 cm^{-1} were assigned to asymmetric and symmetric CH_2 stretching respectively.^{1,2} The peak at 2960 cm^{-1} is most likely due to CH_3 stretching.³ A non H-bonded N-H showed up at 3454 cm^{-1} while H-bonded N-H stretching was at 3236 cm^{-1} . The peak at 3236 cm^{-1} is missing in case of **2** which mean that the molecules are not intermolecularly H-bonded.⁴ The region $1400\text{-}1900\text{ cm}^{-1}$ showed several bands at $1471, 1557, 1577, 1654, 1735\text{ cm}^{-1}$ which were assigned to ferrocene-C stretching, amide I, N-H bending, amide II and C=O stretching respectively.^{4,5,6}

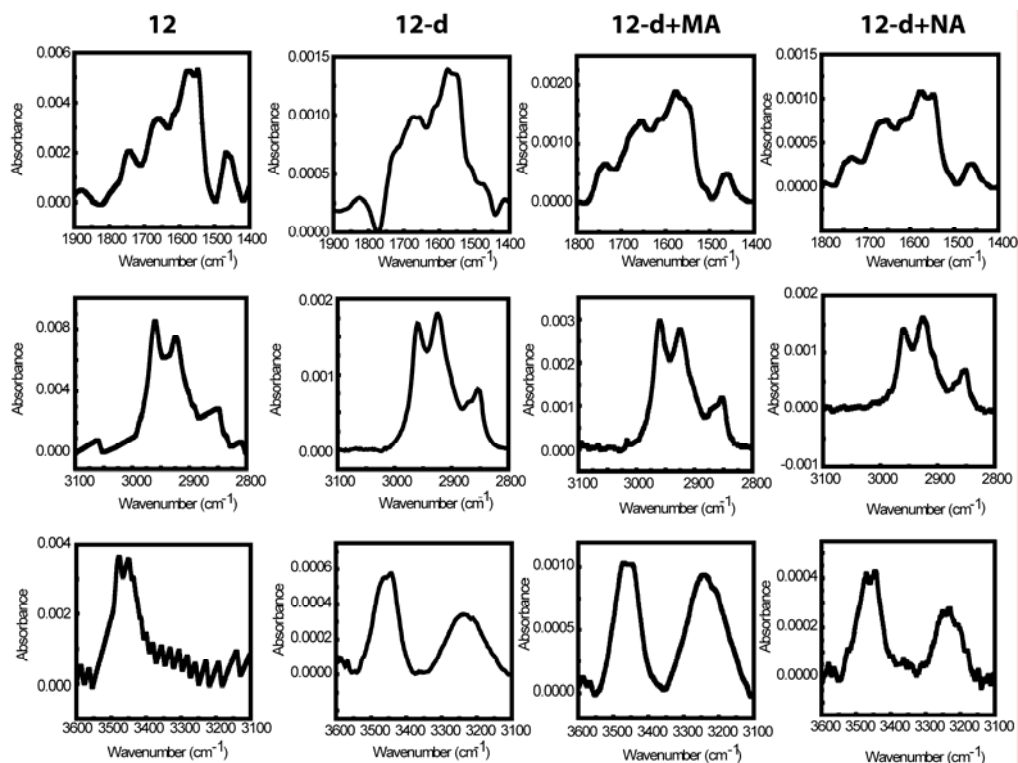


Figure A8. RAIRS spectrum of $[\text{BocNH-Fc-CO-CSA}]_2$ (**12**) on Au surface immobilized by soaking at room temperature from 1 mM ethanolic solution of compound **12**.

- (1) Han, S. W.; Seo, H.; Chung, Y. K.; Kim, K. *Langmuir* **2000**, *16*, 9493-9500.
- (2) Hoffman, H.; Mayer, U.; Brunner, H.; Krischanitz, A. *Vib. Spectrosc.* **1995**, *8*, 151-157.
- (3) Allara, D. L.; Swalen, J. D. *J. Phys. Chem.* **1982**, *86*, 2700-2704.
- (4) Brewer, S. H.; Allen, A. M.; Lappi, S. E.; Chasse, T. L.; Briggman, K. A.; Gorman, C. B.; Franzen, S. *Langmuir* **2004**, *20*, 5512-5520.
- (5) Han, S. W.; Ha, T. H.; Kim, C. H.; Kim, K. *Langmuir* **1998**, *14*, 6113-6120.
- (6) Carter, C.; Brumbach, M.; Donley, C.; Hreha, R. D.; Marder, S. R.; Domercq, B.; Yoo, S.; Kippelen, B.; Armstrong, N. R. *J. Phys. Chem. B* **2006**, *110*, 25191-25202.

Table A1: Interatomic Distances [\AA] for compound **12**

Bond	Distance	Bond	Distance
Fe(1)-C(5)	2.034(3)	S(1)-C(8)	1.804(3)
Fe(1)-C(19)	2.039(3)	S(1)-S(2)	2.0366(13)
Fe(1)-C(1)	2.041(3)	S(2)-C(9)	1.816(3)
Fe(1)-C(20)	2.041(3)	O(1)-C(6)	1.240(3)
Fe(1)-C(4)	2.045(3)	O(2)-C(11)	1.253(3)
Fe(1)-C(21)	2.046(3)	O(3)-C(22)	1.213(4)
Fe(1)-C(3)	2.056(3)	O(4)-C(22)	1.343(3)
Fe(1)-C(2)	2.062(3)	O(4)-C(23)	1.478(4)
Fe(1)-C(18)	2.065(3)	O(5)-C(32)	1.200(4)
Fe(1)-C(17)	2.077(3)	O(6)-C(32)	1.348(4)
Fe(2)-C(12)	2.024(3)	O(6)-C(33)	1.472(4)
Fe(2)-C(16)	2.025(3)	N(1)-C(6)	1.342(4)
Fe(2)-C(30)	2.031(4)	N(1)-C(7)	1.461(4)
Fe(2)-C(13)	2.037(4)	N(2)-C(11)	1.330(4)
Fe(2)-C(29)	2.038(4)	N(2)-C(10)	1.447(4)
Fe(2)-C(27)	2.044(4)	N(3)-C(22)	1.342(4)
Fe(2)-C(31)	2.045(4)	N(3)-C(17)	1.415(4)
Fe(2)-C(28)	2.050(4)	N(4)-C(32)	1.348(4)
Fe(2)-C(15)	2.054(3)	N(4)-C(27)	1.419(4)
Fe(2)-C(14)	2.067(4)	C(12)-C(16)	1.430(4)
C(1)-C(2)	1.420(4)	C(13)-C(14)	1.424(5)
C(1)-C(5)	1.446(4)	C(14)-C(15)	1.409(5)
C(1)-C(6)	1.467(4)	C(15)-C(16)	1.408(4)
C(2)-C(3)	1.419(5)	C(17)-C(18)	1.412(4)
C(3)-C(4)	1.417(5)	C(17)-C(21)	1.422(4)
C(4)-C(5)	1.411(5)	C(18)-C(19)	1.427(4)
C(7)-C(8)	1.525(4)	C(19)-C(20)	1.413(4)
C(9)-C(10)	1.513(4)	C(20)-C(21)	1.422(4)
C(11)-C(12)	1.470(4)	C(23)-C(25)	1.505(5)
C(12)-C(13)	1.419(4)	C(23)-C(24)	1.521(6)
C(23)-C(26)	1.522(5)	C(27)-C(31)	1.429(5)
C(27)-C(28)	1.434(5)	C(28)-C(29)	1.421(6)
C(29)-C(30)	1.414(6)	C(30)-C(31)	1.424(5)
C(33)-C(36)	1.478(6)	C(33)-C(34)	1.496(5)
C(33)-C(35)	1.536(6)	Fe(1)-ct(Cp1)	1.651(1)
Fe(2)-ct(Cp3)	1.646(2)	Fe(1)-ct(Cp2)	1.661(1)
Fe(2)-ct(Cp4)	1.643(2)		

Table A2. Interatomic Angles [°] for compound **12**

	Angle		Angle
C(5)-Fe(1)-C(19)	157.33(13)	C(2)-C(1)-Fe(1)	70.56(17)
C(5)-Fe(1)-C(1)	41.59(11)	C(5)-C(1)-Fe(1)	68.93(16)
C(19)-Fe(1)-C(1)	121.25(12)	C(6)-C(1)-Fe(1)	125.74(19)
C(5)-Fe(1)-C(20)	160.72(12)	C(3)-C(2)-C(1)	108.6(3)
C(19)-Fe(1)-C(20)	40.53(13)	C(3)-C(2)-Fe(1)	69.61(17)
C(1)-Fe(1)-C(20)	156.03(11)	C(1)-C(2)-Fe(1)	68.94(16)
C(5)-Fe(1)-C(4)	40.47(13)	C(4)-C(3)-C(2)	107.8(3)
C(19)-Fe(1)-C(4)	160.94(14)	C(4)-C(3)-Fe(1)	69.37(17)
C(1)-Fe(1)-C(4)	68.71(12)	C(2)-C(3)-Fe(1)	70.08(17)
C(20)-Fe(1)-C(4)	124.13(13)	C(5)-C(4)-C(3)	108.8(3)
C(5)-Fe(1)-C(21)	124.07(11)	C(5)-C(4)-Fe(1)	69.33(16)
C(19)-Fe(1)-C(21)	68.34(11)	C(3)-C(4)-Fe(1)	70.21(17)
C(1)-Fe(1)-C(21)	162.05(12)	C(4)-C(5)-C(1)	107.6(3)
C(20)-Fe(1)-C(21)	40.71(11)	C(4)-C(5)-Fe(1)	70.19(18)
C(4)-Fe(1)-C(21)	107.19(12)	C(1)-C(5)-Fe(1)	69.48(16)
C(5)-Fe(1)-C(3)	68.43(13)	O(1)-C(6)-N(1)	121.3(3)
C(19)-Fe(1)-C(3)	124.52(13)	O(1)-C(6)-C(1)	121.8(3)
C(1)-Fe(1)-C(3)	68.50(13)	N(1)-C(6)-C(1)	116.9(2)
C(20)-Fe(1)-C(3)	107.07(13)	N(1)-C(7)-C(8)	110.8(2)
C(4)-Fe(1)-C(3)	40.42(13)	C(7)-C(8)-S(1)	112.9(2)
C(21)-Fe(1)-C(3)	120.48(13)	C(10)-C(9)-S(2)	111.9(2)
C(5)-Fe(1)-C(2)	68.54(12)	N(2)-C(10)-C(9)	112.1(2)
C(19)-Fe(1)-C(2)	108.19(12)	O(2)-C(11)-N(2)	121.3(3)
C(1)-Fe(1)-C(2)	40.50(12)	O(2)-C(11)-C(12)	120.7(2)
C(20)-Fe(1)-C(2)	120.98(12)	N(2)-C(11)-C(12)	117.9(2)
C(4)-Fe(1)-C(2)	67.81(12)	C(13)-C(12)-C(16)	107.0(3)
C(21)-Fe(1)-C(2)	155.77(13)	C(13)-C(12)-C(11)	128.7(3)
C(3)-Fe(1)-C(2)	40.30(13)	C(16)-C(12)-C(11)	123.9(3)
C(5)-Fe(1)-C(18)	121.75(12)	C(13)-C(12)-Fe(2)	70.03(19)
C(19)-Fe(1)-C(18)	40.70(12)	C(16)-C(12)-Fe(2)	69.34(18)
C(1)-Fe(1)-C(18)	108.16(12)	C(11)-C(12)-Fe(2)	119.7(2)
C(20)-Fe(1)-C(18)	68.30(12)	C(12)-C(13)-C(14)	108.4(3)
C(4)-Fe(1)-C(18)	156.68(13)	C(12)-C(13)-Fe(2)	69.06(19)
C(21)-Fe(1)-C(18)	68.27(12)	C(14)-C(13)-Fe(2)	70.8(2)
C(3)-Fe(1)-C(18)	161.85(13)	C(15)-C(14)-C(13)	107.8(3)
C(2)-Fe(1)-C(18)	125.75(12)	C(15)-C(14)-Fe(2)	69.5(2)
C(5)-Fe(1)-C(17)	108.58(11)	C(13)-C(14)-Fe(2)	68.6(2)

Table A2. Continued....

	Angle		Angle
C(19)-Fe(1)-C(17)	67.38(11)	C(16)-C(15)-C(14)	108.4(3)
C(1)-Fe(1)-C(17)	125.87(12)	C(16)-C(15)-Fe(2)	68.69(18)
C(20)-Fe(1)-C(17)	67.56(12)	C(14)-C(15)-Fe(2)	70.5(2)
C(4)-Fe(1)-C(17)	122.03(12)	C(15)-C(16)-C(12)	108.4(3)
C(21)-Fe(1)-C(17)	40.33(12)	C(15)-C(16)-Fe(2)	70.91(19)
C(3)-Fe(1)-C(17)	156.34(13)	C(12)-C(16)-Fe(2)	69.28(17)
C(2)-Fe(1)-C(17)	162.44(12)	C(18)-C(17)-N(3)	129.4(3)
C(18)-Fe(1)-C(17)	39.85(11)	C(18)-C(17)-C(21)	109.0(3)
C(12)-Fe(2)-C(16)	41.37(12)	N(3)-C(17)-C(21)	121.4(2)
C(12)-Fe(2)-C(30)	153.07(16)	C(18)-C(17)-Fe(1)	69.61(16)
C(16)-Fe(2)-C(30)	164.60(15)	N(3)-C(17)-Fe(1)	131.72(19)
C(12)-Fe(2)-C(13)	40.91(12)	C(21)-C(17)-Fe(1)	68.64(16)
C(16)-Fe(2)-C(13)	68.65(14)	C(17)-C(18)-C(19)	107.1(3)
C(30)-Fe(2)-C(13)	119.49(18)	C(17)-C(18)-Fe(1)	70.54(16)
C(12)-Fe(2)-C(29)	164.24(16)	C(19)-C(18)-Fe(1)	68.67(17)
C(16)-Fe(2)-C(29)	126.67(16)	C(20)-C(19)-C(18)	108.5(2)
C(30)-Fe(2)-C(29)	40.66(19)	C(20)-C(19)-Fe(1)	69.81(17)
C(13)-Fe(2)-C(29)	153.93(16)	C(18)-C(19)-Fe(1)	70.63(16)
C(12)-Fe(2)-C(27)	106.61(13)	C(19)-C(20)-C(21)	108.1(3)
C(16)-Fe(2)-C(27)	118.72(13)	C(19)-C(20)-Fe(1)	69.67(17)
C(30)-Fe(2)-C(27)	68.41(16)	C(21)-C(20)-Fe(1)	69.82(16)
C(13)-Fe(2)-C(27)	126.54(14)	C(17)-C(21)-C(20)	107.3(2)
C(29)-Fe(2)-C(27)	68.36(15)	C(17)-C(21)-Fe(1)	71.03(16)
C(12)-Fe(2)-C(31)	117.88(14)	C(20)-C(21)-Fe(1)	69.47(16)
C(16)-Fe(2)-C(31)	152.99(13)	O(3)-C(22)-N(3)	126.0(3)
C(30)-Fe(2)-C(31)	40.91(15)	O(3)-C(22)-O(4)	125.0(3)
C(13)-Fe(2)-C(31)	107.30(16)	N(3)-C(22)-O(4)	108.9(2)
C(29)-Fe(2)-C(31)	68.82(17)	O(4)-C(23)-C(25)	109.1(3)
C(27)-Fe(2)-C(31)	40.90(15)	O(4)-C(23)-C(24)	110.7(3)
C(12)-Fe(2)-C(28)	125.89(14)	C(25)-C(23)-C(24)	112.0(4)
C(16)-Fe(2)-C(28)	106.99(15)	O(4)-C(23)-C(26)	102.3(3)
C(30)-Fe(2)-C(28)	68.71(19)	C(25)-C(23)-C(26)	110.5(4)
C(13)-Fe(2)-C(28)	164.17(14)	C(24)-C(23)-C(26)	111.8(4)
C(29)-Fe(2)-C(28)	40.68(16)	N(4)-C(27)-C(31)	127.1(3)
C(27)-Fe(2)-C(28)	41.00(15)	N(4)-C(27)-C(28)	124.1(3)
C(31)-Fe(2)-C(28)	69.27(17)	C(31)-C(27)-C(28)	108.8(3)
C(12)-Fe(2)-C(15)	68.75(13)	N(4)-C(27)-Fe(2)	125.6(2)

Table A2. Continued....

	Angle		Angle
C(16)-Fe(2)-C(15)	40.39(13)	C(31)-C(27)-Fe(2)	69.6(2)
C(30)-Fe(2)-C(15)	127.63(15)	C(28)-C(27)-Fe(2)	69.7(2)
C(13)-Fe(2)-C(15)	68.07(14)	C(29)-C(28)-C(27)	106.9(4)
C(29)-Fe(2)-C(15)	108.61(16)	C(29)-C(28)-Fe(2)	69.2(2)
C(27)-Fe(2)-C(15)	153.33(15)	C(27)-C(28)-Fe(2)	69.3(2)
C(31)-Fe(2)-C(15)	164.90(15)	C(30)-C(29)-C(28)	108.7(3)
C(28)-Fe(2)-C(15)	119.16(16)	C(30)-C(29)-Fe(2)	69.4(2)
C(12)-Fe(2)-C(14)	68.60(13)	C(28)-C(29)-Fe(2)	70.1(2)
C(16)-Fe(2)-C(14)	67.91(14)	C(29)-C(30)-C(31)	108.8(4)
C(30)-Fe(2)-C(14)	108.90(17)	C(29)-C(30)-Fe(2)	69.9(2)
C(13)-Fe(2)-C(14)	40.60(13)	C(31)-C(30)-Fe(2)	70.1(2)
C(29)-Fe(2)-C(14)	120.07(15)	C(30)-C(31)-C(27)	106.8(4)
C(27)-Fe(2)-C(14)	164.80(15)	C(30)-C(31)-Fe(2)	69.0(2)
C(31)-Fe(2)-C(14)	127.34(16)	C(27)-C(31)-Fe(2)	69.53(19)
C(28)-Fe(2)-C(14)	153.41(15)	O(5)-C(32)-O(6)	126.4(3)
C(15)-Fe(2)-C(14)	39.99(14)	O(5)-C(32)-N(4)	124.9(3)
C(8)-S(1)-S(2)	102.03(12)	O(6)-C(32)-N(4)	108.6(3)
C(9)-S(2)-S(1)	102.55(12)	O(6)-C(33)-C(36)	110.4(3)
C(22)-N(3)-C(17)	125.4(2)	O(6)-C(33)-C(34)	110.2(3)
C(32)-N(4)-C(27)	122.9(3)	C(36)-C(33)-C(34)	114.1(5)
C(2)-C(1)-C(5)	107.1(3)	O(6)-C(33)-C(35)	101.2(3)
C(2)-C(1)-C(6)	124.8(3)	C(36)-C(33)-C(35)	111.2(5)
C(5)-C(1)-C(6)	128.1(3)	C(34)-C(33)-C(35)	109.1(4)

Copy right permission from Elsevier for Figure 1.1



Dear Mr. Khan,

We hereby grant you permission to reprint the aforementioned material at no charge **in your thesis, in print and on the University of Saskatchewan web site** subject to the following conditions:

1. If any part of the material to be used (for example, figures) has appeared in our publication with credit or acknowledgement to another source, permission must also be sought from that source. If such permission is not obtained then that material may not be included in your publication/copies.
2. Suitable acknowledgment to the source must be made, either as a footnote or in a reference list at the end of your publication, as follows: “Reprinted from Publication title, Vol number, Author(s), Title of article, Pages No., Copyright (Year), with permission from Elsevier”.
3. Your thesis may be submitted to your institution in either print or electronic form.
4. Reproduction of this material is confined to the purpose for which permission is hereby given.
5. This permission is granted for non-exclusive world **English** rights only. For other languages please reapply separately for each one required. Permission excludes use in an electronic form. Should you have a specific electronic project in mind please reapply for permission.
6. This includes permission for the Library and Archives of Canada to supply single copies, on demand, of the complete thesis. Should your thesis be published commercially, please reapply for permission.

Yours sincerely



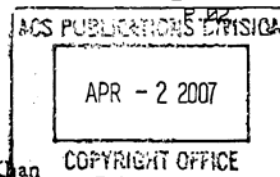
Manuela Beis
Rights Assistant

Copy right permission from American Chemical Society (ACS) for Figure 1.2 – 1.6 and Scheme 1.6

/2007 14:26 FAX 2027768112
-29-2007 14:43

002/002

PERMISSION REQUEST FORM



Date: March 29, 2007

To: Copyright Office
Publications Division
American Chemical Society
1155 Sixteenth Street, N.W.
Washington, DC 20036

From: Mohammad Abdul Kader Khan
110 Science Place, Department of Chemistry
University of Saskatchewan, Saskatoon
Saskatchewan, Canada S7N 5C9

FAX: 202-776-8112

Your Phone No. 1-306-966-1636; 1-306-966-4712
Your Fax No. 1-306-966-4730

I am preparing a paper entitled:

Electrochemical Detection of Chemical Warfare Agents

to appear in a (circle one) book, magazine, journal, proceedings, other: Thesis
entitled: **Electrochemical Detection of Chemical Warfare Agents** to be published by:

Department of Chemistry, University Of Saskatchewan

I would appreciate your permission to use the following ACS material in print and other formats with the understanding that the required ACS copyright credit line will appear with each item and that this permission is for only the requested work listed above:

From ACS journals or magazines (for ACS magazines, also include issue no.):

ACS Publication Title	Issue Date	Vol.No.	Page(s)	Material to be used*
Analytical Chemistry	6, March 15, 1998	70	1085 - 1091	Figure 6
Analytical Chemistry	11, June 1, 1999	71	2246 - 2249	Figure 1 & 4
Analytical Chemistry	3, January 1, 2006	78	835 - 843	Figure 1,8 & 10
Analytical Chemistry	10, May 15, 2004	76	2689 - 2693	Scheme 1 & Figure 4
Analytical Chemistry	18, Sept. 15, 2005	77	5894-5901	Figure 2

From ACS books: include ACS book title, series name and number, year, page(s), book editor=s name(s), chapter author's name(s), and material to be used, such as Figs. 2 & 3, full text, etc.*

* If you use more than three figures/tables from any article and/or chapter, the author's permission will also be required.

Questions? Please call Arleen Courtney at (202) 872-4368 or use the FAX number above.

This space is reserved for
ACS Copyright Office Use

PERMISSION TO REPRINT IS GRANTED BY
THE AMERICAN CHEMICAL SOCIETY

ACS CREDIT LINE REQUIRED. Please follow this sample:
Reprinted with permission from (reference citation). Copyright
(year) American Chemical Society.

APPROVED BY: C. Arleen Courtney 4/3/07
ACS Copyright Office

If box is checked, author permission is also required. See original article for address.

12/3/99

TOTAL P.02